Potential performance for Pb-Pb, *p*-Pb, and *p*-*p* collisions in a future circular collider

Michaela Schaumann[*]

CERN, CH-1211 Geneva 23, Switzerland and III. Physikalisches Institut,
RWTH Aachen University, D-52056 Aachen, Germany

The hadron collider studied in the future circular collider (FCC) project could operate with protons and lead ions in similar operation modes as the LHC. In this paper the potential performances in lead-lead, proton-lead, and proton-proton collisions are investigated. Based on average lattice parameters, the strengths of intrabeam scattering and radiation damping are evaluated and their effect on the beam and luminosity evolution is presented. Estimates for the integrated luminosity per fill and per run are given, depending on the turnaround time. Moreover, the beam-beam tune shift and bound free pair production losses in heavy-ion operation are addressed.

I. MOTIVATION

The future circular collider (FCC) is a recently proposed collider study in a new 80–100 km tunnel at CERN in the Geneva area [1]. The design study includes three collider options: FCC-ee (formerly known as TLEP), a e^+e^- collider with a center-of-mass energy of 90–400 GeV, seen as a potential intermediate step; FCC-hh, a hadron collider with a center-of-mass energy of the order of 100 TeV in proton-proton collisions as a long-term goal; and FCC-he, combining both as a hadron-electron collider.

The beam energy of the hadron machine is expected to be $E_b = 50Z$ TeV, where Z is the charge number of the circulating nuclei. Its main purpose will be to search for new physics in energy regimes which have never been reached before. The FCC-hh will therefore spend most of its physics time providing proton-proton collisions to its experiments. Nevertheless, operating this machine with heavy ions is being considered. It would provide, for example, Pb-Pb and *p*-Pb collisions at $\sqrt{s_{NN}} = 39$ and 63 TeV, respectively. From the heavy-ion physics point of view, using the FCC-hh as a heavy-ion collider would open a whole new regime of research opportunities [2].

This paper discusses potential FCC-hh beam parameters for heavy-ion operation. The dominating beam dynamic effects and estimates for the time evolution of luminosity, intensity, emittances and bunch length by analytic equations and collider time evolution (CTE) [3] simulations are presented. An approximated smooth lattice model is assumed. Lead-lead (Pb-Pb) and proton-lead (*p*-Pb)

operation are considered. We close with a short discussion of proton-proton (*p*-*p*) operation, based on the same techniques.

II. GENERAL ASSUMPTIONS

It is foreseen to operate the FCC-hh with different types of particles, e.g., protons (*p*) and lead-ions (Pb), but potentially also other ion species. The choice of certain parameters and hardware components has to ensure the compatibility with all potential beams. As mentioned, the production of *p*-*p* collisions will be the main task, restricting the heavy-ion run time to a few weeks per year, similar to the current Large Hadron Collider (LHC) schedule. In order to optimize time and cost, the operation with different species should share mostly the same equipment and machine settings should be kept as similar as possible. For this reason, the parameters to be chosen for the heavy-ion operation are in line with those for *p*-*p* operation documented in [4], where possible. Considering superconducting magnets based on Nb$_3$Sn with a field strength of 16 T, the same arc filling factor (i.e., the fraction of the arc that can be filled with dipoles) as in the LHC of 79% and scaling the length of all straight sections to about 4 times that of the LHC (i.e., in total 16.8 km), the required circumference of the accelerator to provide a maximum beam energy of $E_b = 50Z$ TeV sums up to about $C_{ring} = 100$ km. Details on these parameter choices can be found in Ref. [4]. This work assumes the just quoted parameter option as a baseline for all calculations presented.

A. Preaccelerator chain

The study of this new hadron collider began only recently and the requirements for the preaccelerator chain are still undefined. Assuming the same ratio of injection to full energy as for the LHC, the injection energy of the FCC-hh would be $E_{b,inj} = 3.3Z$ TeV.

[*]Michaela.Schaumann@cern.ch

Taking the existing CERN infrastructure into account, Ref. [4] tentatively suggests three options for the last accelerator injecting into the FCC: a machine built either in the super proton synchrotron (SPS), the LHC or the FCC tunnel. The magnet strength required for an injection energy of 3.3Z TeV would be 1 T, for an injector with normal conducting magnets in the 100 km FCC tunnel. 3.6 T, using superconducting LHC-type magnets (Nb-Ti) in the existing LHC tunnel. 13.5 T, using Nb_3Sn magnets replacing the SPS. A choice has not been made, but using the existing superconducting LHC magnets seems to be the most favored and cost effective option today. Equipping the LHC magnets with new power converters and ramping to only about half their maximum field could reduce the ramp time to an acceptable value of a few minutes.

Based on this, it will be assumed here that the existing preaccelerator complex, including the LHC, is used to accelerate the particles up to 3.3Z TeV before injection into the new ring. Both LHC rings are filled and the beams are injected in opposite direction into the FCC. This is a reliable but conservative assumption. Major upgrades are essential in the injector chain to satisfy the requirements of the FCC experiments and to obtain a realistic filling time. The heavy-ion program will benefit from the efforts made. It can be expected that the performance and turnaround time will be significantly improved compared to the current situation, but the amount of improvement would be speculative today.

B. Smooth lattice approximation

At the time of this study, the lattice design is still preliminary [5]. However, for the calculation of many parameters and effects, the knowledge of certain lattice properties is required. In the design of a new machine, one has to respect some constraints, from which at least a first approximation of the range of these quantities can be derived.

As a baseline it is assumed that the lattice would be a similar FODO design (F = focusing, D = defocusing, O = zero focusing) as in the LHC. The maximum (and minimum) β-function in a FODO cell is directly proportional to the cell length, L_c [6]:

$$\beta^{\pm} = \frac{L_c(1 \pm \sin\frac{\mu}{2})}{\sin\mu} \propto L_c, \qquad (1)$$

where μ is the phase advance per cell. To keep the beam size in the arcs at a reasonable value, L_c should not exceed twice the LHC value of $L_{c,\mathrm{LHC}} = 106.9$ m. It seems adequate to investigate cell lengths between one and two times the LHC value. A tendency to the upper range, close to $2L_{c,\mathrm{LHC}}$, seems to be favored as a compromise between magnet aperture and strength.

To obtain an expression for the average β-function, $\langle\beta\rangle$, which is used in the intrabeam scattering (IBS) calculations below, the phase advance per cell, μ, is approximated [7]:

$$\mu \equiv \int_0^{L_c} \frac{ds}{\beta(s)} \approx \frac{1}{\langle\beta\rangle} \int_0^{L_c} ds = \frac{L_c}{\langle\beta\rangle}. \qquad (2)$$

The horizontal dispersion is produced in the bending magnets and is therefore proportional to the bending angle per cell, θ_c, times L_c. The average dispersion in a FODO cell, $\langle D_x \rangle$, is given by [6]:

$$\langle D_x \rangle = \frac{L_c\theta_c}{4}\left(\frac{1}{\sin^2\frac{\mu}{2}} - \frac{1}{12}\right) \propto L_c\theta_c. \qquad (3)$$

The total bending angle of the ring, the sum over $\theta_{c,i}$ of all cells, is 2π:

$$2\pi = \Sigma\theta_{c,i} = N_c\theta_c \Rightarrow \theta_c = \frac{2\pi}{N_c},$$

where N_c is the total number of FODO cells in the ring. The length of the circumference, filled by the arcs, is

$$L_{\mathrm{arcs}} = N_cL_c = \frac{2\pi}{\theta_c}L_c.$$

Of this length, the dipoles themselves only occupy the fraction F_{arc}, giving:

$$L_{\mathrm{dipole}} = 2\pi\rho_0 = F_{\mathrm{arc}}L_{\mathrm{arcs}} = F_{\mathrm{arc}}\frac{2\pi}{\theta_c}L_c,$$

with ρ_0 as the dipole bending radius. It follows that the average horizontal dispersion is related to the cell length as:

$$\theta_cL_c = L_c^2\frac{F_{\mathrm{arc}}}{\rho_0} \propto L_c^2 \qquad (4)$$

$$\Leftrightarrow \langle D_x \rangle \propto L_c^2. \qquad (5)$$

The vertical dispersion is in general very small and corrected for. Therefore, it is assumed to be zero:

$$\langle D_y \rangle = 0.$$

Assuming a phase advance of $\mu = \pi/2$ per cell and an arc filling factor of $F_{\mathrm{arc}} = 0.79$, as in the LHC, Eq. (1), (2), (3), and (4) can be used to express the dispersion and β-functions in terms of the cell length L_c.

The choice of the phase advance per cell is based on the LHC, which has arc cells featuring approximately 90° phase advance per cell in both planes. The deviation of the LHC cells from 90° is necessary to correct the systematic coupling generated by the main dipole field errors, which favors an optics with an integer tune split between the horizontal and vertical tunes [8]. These effects are not yet taken into account for this study and the average phase advance (equal to $\mu = \pi/2$) is assumed in both planes.

Choosing another value for the phase advance could improve the IBS [9]. Given that IBS in this machine is relatively unimportant compared to LHC (as discussed in the next chapter), the achievable gain would not be worth pursuing another phase advance.

The momentum compaction factor, α_c, and the relativistic gamma factor at transition energy, γ_T, can be approximated via the average horizontal dispersion:

$$\alpha_c \equiv \frac{1}{\gamma_T^2} = \frac{1}{C_{\mathrm{ring}}} \oint \frac{D_x}{\rho_0} ds \approx \frac{2\pi \langle D_x \rangle}{C_{\mathrm{ring}}}. \tag{6}$$

C. Beam parameters

The potential beam parameter space is constrained by many different limitations, including the injector performance and dynamic effects in the whole operational cycle. The beam parameters presented in the following are an example of what could be possible from today's knowledge. Further studies should be performed to confirm their validity and to determine the optimum parameter set.

Using the existing preaccelerator chain, it can be expected that beam parameters at least as good as in the LHC can be achieved. For the moment, the bunch-by-bunch differences observed in LHC operation [10] are neglected. Average bunch parameters measured in the 2013 proton-lead run [11,12] are taken as a conservative baseline. The assumed beam parameters for the lead and proton beams for heavy-ion operation of the FCC-hh are given in Table I.

For the number of bunches per beam, k_b, given in Table I, one injection per beam from the LHC is assumed. The LHC filling is assumed to be the planned "baseline" filling scheme after LS2 [13]. One shot from the LHC fills only about one quarter of the total circumference of the FCC. This implies that either only one experiment, clusters of experiments or two experiments, placed at opposite positions in the ring, could be provided with collisions. The reason for this choice is related to the turnaround time of the LHC as an injector, which will be explained in the discussion of the luminosity evolution. The β^*-values are the same as during *p*-*p* operation.

Intensity losses and emittance growth at injection, during the ramp and while preparing collisions are neglected.

TABLE I. Assumed beam parameters for heavy-ion operation in Pb-Pb and *p*-Pb collisions.

Parameter	Symbol	Unit	Lead	Proton
Number of particles per bunch	N_b	[10^8]	1.4	115
Normalized transverse emittance	ϵ_n	[μm]	1.5	3.75
rms bunch length	σ_s	[m]	0.08	0.08
Number of bunches per beam	k_b	$\cdots$	432	432
β-function at IP	β^*	[m]	1.1	1.1

D. rf system and longitudinal parameters

A rf system similar to the one currently used in the LHC, which has a frequency of $f_{\mathrm{rf}} = 400.8$ MHz, gives an harmonic number of

$$h = \frac{f_{\mathrm{rf}}}{f_{\mathrm{rev}}} = 133692 (= 2^2 \times 3 \times 13 \times 857)$$

in a ring with a circumference of exactly $C_{\mathrm{ring}} = 100$ km. In reality, the circumference will be adjusted to give an h with more small factors, but this is not important in the following.

1. Injection

When the beam is injected, assuming bunch to bucket transfer, the longitudinal beam parameters, i.e., the relative rms momentum spread, σ_p, the rms bunch length, σ_s, and the longitudinal emittance, ϵ_s, are defined by the previous accelerator. To conserve the beam quality, the rf bucket has to be matched to the arriving beam. Assuming an injected bunch length of $\sigma_s = 0.1$ m, the corresponding σ_p and ϵ_s arriving from the LHC can be calculated as

$$\sigma_p = 2\pi \frac{f_s \sigma_s}{c|\eta|} = 1.9 \times 10^{-4}, \tag{7}$$

$$\epsilon_s = 4\pi \sigma_p \sigma_s \beta_{\mathrm{rel}} E_b / (Zc) = 2.6 \text{ eVs/charge}, \tag{8}$$

where f_s is the synchrotron frequency given by

$$f_s = f_{\mathrm{rev}} \sqrt{\frac{|\eta| V_{\mathrm{rf}} h Z e}{2\pi \beta_{\mathrm{rel}} E_b}}, \tag{9}$$

with f_{rev} as the revolution frequency, $\beta_{\mathrm{rel}} = v/c$ and E_b as the energy of the synchronous particle. $\eta = \frac{1}{\gamma_T^2} - \frac{1}{\gamma^2}$ is the slip factor with γ as the relativistic Lorentz factor, Ze the particles' charge. At $E_b = 3.3Z$ TeV, an rf voltage of $V_{\mathrm{rf}} = 12$ MV was used in the LHC.

From Eq. (8), it follows that ϵ_s is constant, if σ_s and σ_p are constant. If σ_s can be preserved during the transfer, Eqs. (7) and (9) show that for a given lattice the rf voltage is the only free parameter to match the momentum spread.

Because of the preliminary stage of the lattice design, the effect of a varying cell length should be investigated. γ_T is the only parameter in Eq. (7) depending on the lattice. From Eq. (6), (3), and (5) follows

$$\gamma_T \propto \frac{1}{L_c} \Rightarrow \sigma_p \propto \gamma_T \sqrt{V_{\mathrm{rf}}} \propto \frac{\sqrt{V_{\mathrm{rf}}}}{L_c} \tag{10}$$

for $\gamma \gg \gamma_T$. To obtain a matched distribution with σ_p equal to the injected value, V_{rf} has to be increased proportionally to the square of the cell length as shown in Fig. 1.
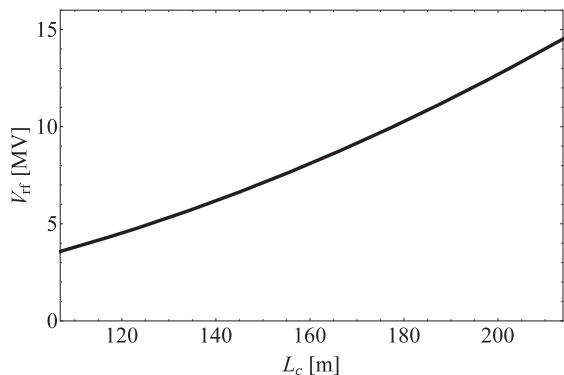
FIG. 1.   rf voltage dependence on lattice at injection in the FCC for matched bucket condition.

FIG. 2.   rms momentum spread dependence on lattice and rf voltage at top energy, as described by Eq. (10).

We define a baseline FCC-hh lattice with a FODO cell length of $L_c \approx 203$ m and a phase advance per cell of $\mu = \pi/2$ for the calculations in the following. With this, Eq. (3) and (6) estimate $\gamma_T \approx 103$. Equation (2) gives $\langle \beta \rangle \approx 129$ m. Figure 1 shows that for this baseline lattice, an rf voltage of about $V_{rf} = 13$ MV is required at injection in the FCC.

2. Top Energy

To counteract the adiabatic damping of the bunch length during the energy ramp, white rf noise is applied to keep σ_s at a constant value of 0.08 m. This value is taken from the p-p parameter list and is based on the need of the experiments to resolve primary vertices within one bunch crossing, imposing a minimum length of the luminous region [4].

Using an rf voltage of $V_{rf} = 32$ MV, twice the LHC design value [8], at top energy of the FCC-hh, the synchrotron frequency, the relative rms momentum spread and the longitudinal emittance are

$$f_s = 3.4 \text{ Hz},$$

$$\sigma_p = 0.6 \times 10^{-4},$$

$$\epsilon_s = 10.1 \text{ eVs/charge}.$$

The bucket height, $(\Delta p/p)_{max}$, and area, A_{bucket}, evaluate to [6]

$$\left(\frac{\Delta p}{p}\right)_{max} = \sqrt{\frac{2 \, Z e V_{rf}}{\pi h |\eta| \beta_{rel} E_b}} = 1.8 \times 10^{-4},$$

$$A_{bucket} = \frac{8 C_{ring}}{h \pi c} \sqrt{\frac{Z e V_{rf} E_b}{2 \, \pi h |\eta|}} = 28.6 \text{ eVs/charge}.$$

At injection energy these values are $(\Delta p/p)_{max} = 4.5 \times 10^{-4}$ and $A_{bucket} = 4.7$ eVs/charge. The calculation is based on the baseline lattice defined in the previous paragraph.
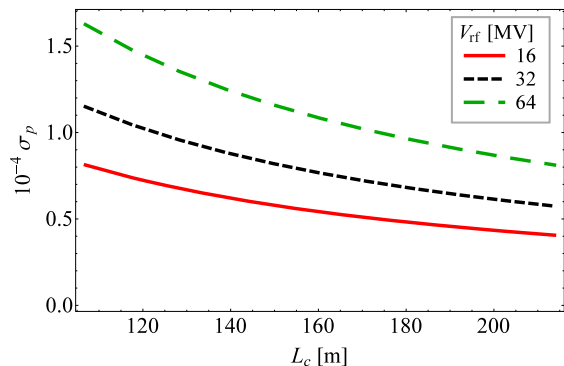
An energy spread of 0.6×10^{-4} seems small and it has to be investigated in detail, if this would cause instabilities. As Eq. (10) states and Fig. 2 visualises, increasing the rf voltage could be advantageous, but the gain in σ_p is small for L_c on the order of twice the LHC cell length. In the design stage of the machine, it could as well be an option to increase γ_T by decreasing the cell length to obtain a higher σ_p. Nevertheless, the benefit has to be weighed against other design criteria relying on the cell length. For a chosen bunch length, the longitudinal emittance will behave proportionally to the momentum spread.

In general, it seems reasonable to aim for a similar momentum spread as in the LHC, around $\sigma_p = 1.1 \times 10^{-4}$. This however would require an extremely high rf voltage of about $V_{rf} \approx 100$ MV.

III. LEAD-LEAD OPERATION

Based on the assumptions made above, approximations of relevant beam properties and effects are calculated in the following section. Because of the preliminary state of the accelerator design, simplifying assumptions had to be made in several places, therefore the study presented here can only give a first indication of what could be expected from heavy-ion operation of such a machine.

A. Intrabeam scattering

Intrabeam scattering (IBS) is a dynamic effect within a bunch of charged particles, where multiple small-angle Coulomb scattering leads to particle losses and emittance growth. This effect can become very strong and reduce the potential luminosity (see, e.g., [10,14]).

1. Formalism and scaling

Several formalisms are available describing the physical effects derived by Piwinski, Bjorken, and Mitingwa, Bane, Nagaitsev or Wei [15–19], based on different assumptions and suitable for different situations. To estimate the effect in the FCC-hh, the methods of Piwinski [15] and Wei [19] are used.

Piwinski's equations for the IBS emittance growth rates, α_{IBS}, can be found in [20]. In his formalism the α_{IBS} are proportional to

$$A_{\text{p}} = \frac{2r_0^2 N_b m_0 c^2}{16\pi\gamma\epsilon_{n,x}\epsilon_{n,y}(Z\epsilon_s)}, \tag{11}$$

where ϵ_s is the invariant longitudinal emittance per charge given by Eq. (8), $\epsilon_{n,xy} = \beta_{\text{rel}}\gamma\epsilon_{xy}$ are the transverse normalized emittances, r_0 the classical particle radius, which relates to the classical proton radius, r_{p0}, as $r_0 = Z^2/A_{\text{ion}}r_{p0}$, and m_0 is the rest mass of the particle. This factor gives an indication of the scaling and quantities most important for the IBS strength. Equation (11) scales inversely with the energy, meaning the IBS growth is strongly suppressed at higher energies. On the other hand, the rates increase with bunch intensity and decrease with growing emittances [$\alpha_{\text{IBS}} \propto N_b/(\epsilon_{n,x}\epsilon_{n,y}\epsilon_s)$], implying that the higher the bunch brightness, desired for luminosity production, the stronger the IBS. A third relevant proportionality is the relation to r_0, which depends on the particles' mass and charge ($\alpha_{\text{IBS}} \propto Z^2/A_{\text{ion}}$), hence the effect is stronger for heavy ions compared to protons. The remaining factors in Piwinski's equations are complicated and depend mainly on lattice parameters, like the dispersion and β-functions, and the beam divergences in all dimensions.

In a simplified formalism J. Wei derived analytical equations of the IBS emittance growth rates of hadron beams [19], provided that the lattice of the accelerator mainly consists of regular FODO cells. For full coupling between the horizontal and vertical motion, the growth rates average in the transverse dimension. For round beams ($\epsilon = \epsilon_x = \epsilon_y$) and if the motion is fully coupled, Wei's formulas for the IBS emittance growth rates are

$$\alpha_{\text{IBS},x,y} = \frac{C_1 N_b}{\sigma_s \epsilon^2 \sqrt{\epsilon + C_2 \sigma_p^2}} \tag{12}$$

$$\alpha_{\text{IBS},s} = \frac{C_3 \epsilon}{\sigma_p^2} \alpha_{\text{IBS},x,y}, \tag{13}$$

where C_1, C_2, and C_3 are constant during operation:

$$C_1 = \frac{5\sqrt{2}cZ^4 r_{p0}^2}{8A_{\text{ion}}^2\gamma^5\beta_{\text{rel}}^3}\frac{2D_x^2\gamma^2 - \beta_x(\beta_x + \beta_y)}{\beta_x\sqrt{\beta_x + \beta_y}}$$

$$C_2 = \frac{D_x^2}{\beta_x}$$

$$C_3 = \frac{4\gamma^2\beta_x}{2D_x^2\gamma^2 - \beta_x(\beta_x + \beta_y)}.$$

Following the smooth lattice approximation, the average of the dispersion and β-functions of Eqs. (3) and (2) are used in the IBS equations. In this form the longitudinal and transverse growth rates are directly related.

2. Calculation of IBS growth rates

The large parameter space, originating from the uncertainties of the lattice design, defines a range of IBS growth rates. Equations (2) and (3) are used to estimate the average dispersion, $\langle D_x \rangle$, and β-functions, $\langle \beta_{x,y} \rangle$, required to approximate the IBS growth rates.

Figure 3 shows $1/\alpha_{\text{IBS}}$ as a function of L_c at (a) 3.3Z TeV (injection energy) and at (b, c) 50Z TeV (collision energy) for the initial bunch parameters given in Table I. Only the longitudinal and horizontal plane are shown. IBS in the vertical plane is negligible without coupling, as assumed in the calculations. For the plots at top energy the dependence of σ_p on L_c is taken into account, while σ_p is constant at injection energy. The results are calculated for a set of rf voltages. σ_p can become very small for long cells (Fig. 2) and larger rf voltage can mitigate this effect.

Note that the horizontal IBS strength increases (= decreasing $1/\alpha_{\text{IBS}}$) and the longitudinal decreases with increasing L_c at injection, but at top energy both, $\alpha_{\text{IBS},s}$ and $\alpha_{\text{IBS},x}$, become stronger for longer cells. The factors in the IBS calculation depending on the cell length are $\langle D_x \rangle \propto L_c^2$, $\langle \beta_x \rangle \propto L_c$ and $\sigma_p \propto 1/L_c$. If σ_p is independent of L_c (as in the case of the injected beam), $\alpha_{\text{IBS},s}$ only has a weak dependence on the lattice, while $\alpha_{\text{IBS},x}$ features a second term $\propto D_x^2 \propto L_c^4$ [20]. At top energy, σ_p is influenced by the lattice conditions and becomes a function of L_c. Thus the strong dependence of $\alpha_{\text{IBS},s}$ on σ_p takes over and the longitudinal IBS growth is enhanced for long cells.

In general, IBS could lead to longitudinal emittance growth at injection energy, while the transverse growth rates are moderate. At collision energy IBS should still be modest, with growth times above 20 h. The situation even improves, if the energy spread could be kept at the LHC design value, see Table II.

However, as it will be shown in the next section, this is only true for the initial beam parameters right after arriving at top energy. Because of the strong radiation damping, the beam emittances will shrink and the IBS will become strong enough to balance the damping.

Table II summarizes the IBS growth times for a bunch with initial parameters, assuming (a) $\sigma_p = 0.6 \times 10^{-4}$ (obtained with γ_T of baseline lattice) and (b) $\sigma_p = 1.1 \times 10^{-4}$ (LHC design) at collision energy, $\sigma_p = 1.9 \times 10^{-4}$ at injection energy. The dispersion and β-functions are taken as calculated from the baseline lattice with $L_c = 203$ m. The comparison of the formalisms by Piwinski and Wei shows that Wei estimates a systematically slightly stronger IBS rate. The overall agreement is better than 10% at high energy and 20% at injection energy for the given parameters.
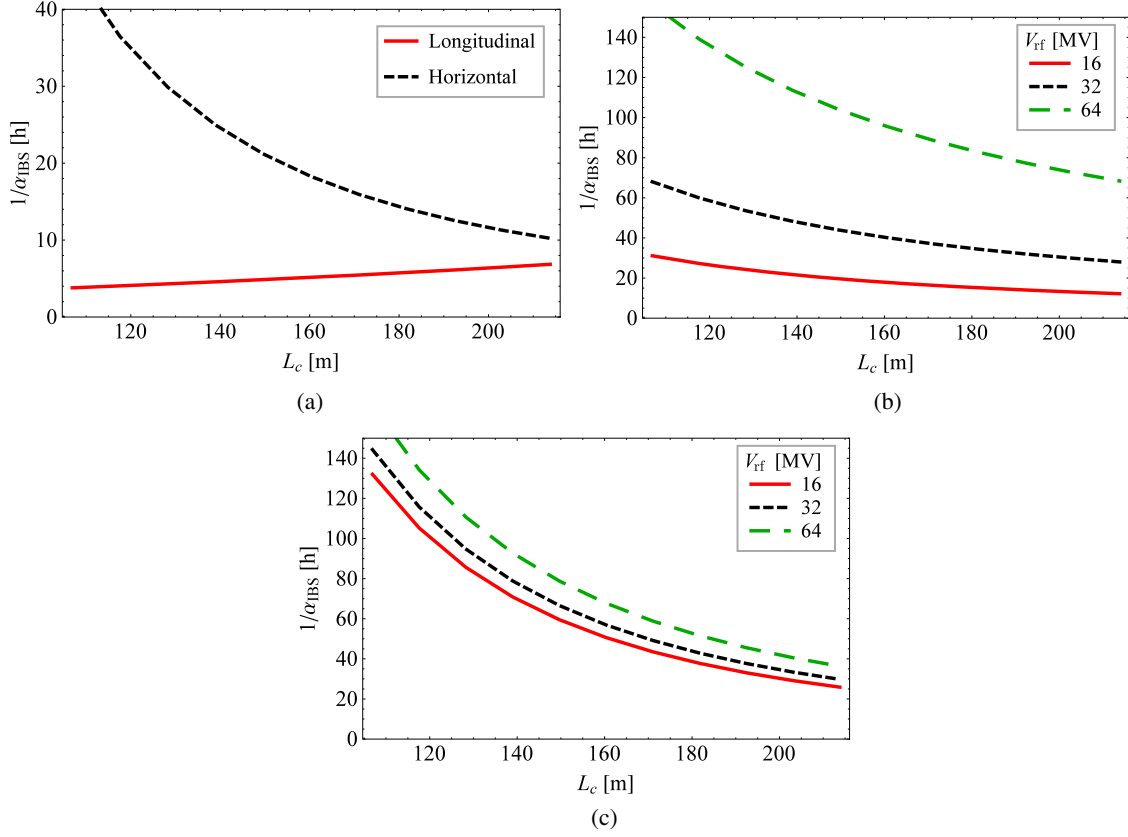
FIG. 3.   Range of initial IBS growth times as a function of the cell length, L_c, at injection (a) and collision (b, c) energy, evaluated with Piwinski's equations [20]. (b) longitudinal, (c) horizontal growth times. For given values of the total rf voltage, V_{RF}. No transverse coupling assumed.

B. Radiation damping

A charged particle traveling in a storage ring will radiate energy, when it is bent on its circular orbit. Because of the average energy loss into this synchrotron radiation, the betatron and synchrotron oscillation amplitudes are damped like $A_i = A_{0,i}e^{-\alpha_i t}$, where $i = x, y, s$, with the radiation damping rates α_i given in Chapter 3.1.4 of [6].

For a flat, isomagnetic ring with separated function magnets and zero vertical dispersion, the radiation emittance damping rates can be approximated by

$$\alpha_{\mathrm{rad},s} = 2\alpha_{\mathrm{rad},x,y} \approx 2E_b^3 C_\alpha \frac{4\pi}{\rho_0 C_{\mathrm{ring}}}, \qquad (14)$$

where $C_\alpha = r_0 c/(3(m_{\mathrm{ion}}c^2)^3)$. Those quantities do not depend on the beam parameters. The strongest dependence is on the third power of the energy, the machine size and the particle type. Note that the longitudinal damping is twice as fast as the transverse.

To get an impression how strong the radiation damping will be in the FCC, the damping rates are compared to the LHC design values:

TABLE II.   Initial IBS growth times for Pb-ions calculated with the Piwinski [20] and Wei [19] formulas, assuming baseline lattice ($L_c = 203$ m) and no transverse coupling. Assumption for momentum spread: injection $\sigma_p = 1.9 \times 10^{-4}$ at $V_{\mathrm{rf}} = 13$ MV, collision (a) $\sigma_p = 0.6 \times 10^{-4}$ (obtained with γ_T of baseline lattice), (b) $\sigma_p = 1.1 \times 10^{-4}$ (LHC design) at $V_{\mathrm{rf}} = 32$ MV.

Growth Times	Unit	Injection		Collision			
				(a)		(b)	
		Piwinski	Wei	Piwinski	Wei	Piwinski	Wei
$1/\alpha_{\mathrm{IBS},s}$	[h]	6.5	5.2	29.9	27.9	143.3	133.3
$1/\alpha_{\mathrm{IBS},x}$	[h]	11.2	9.1	33.4	31.1	48.3	45.0
$1/\alpha_{\mathrm{IBS},y}$	[h]	-10^4	-10^3	-10^6	-10^6	-10^6	-10^6

TABLE III.   Emittance radiation damping times for Pb-ions.

Damping times	Unit	Injection	Collision
$1/\alpha_{\rm rad,s}$	[h]	852	0.24
$1/\alpha_{\rm rad,x}$	[h]	1704	0.49
$1/\alpha_{\rm rad,y}$	[h]	1704	0.49

$$\frac{\alpha_{\rm rad,FCC}}{\alpha_{\rm rad,LHC}} \approx \frac{E_{\rm FCC}^3/C_{\rm FCC}^2}{E_{\rm LHC}^3/C_{\rm LHC}^2} \approx \frac{7^3}{4^2} \approx 22.$$

This scaling is valid for all planes, because of relation (14). The circumference of the accelerator was chosen such that the required dipole field does not exceed the expected technical limits. Therefore, the bending radius can be approximated to be proportional to the circumference, $\rho_0 \propto C_{\rm ring}$. The new machine will be about a factor 4 longer than the LHC. Moreover, the energy will be increased by about a factor 7 ($= 50Z$ TeV/7Z TeV). Table III quotes the radiation damping times at injection and collision energy. Note that the horizontal equilibrium emittance from quantum excitation for lead beams at top energy is of the order of 10^{-5} μm, the effect is thus still negligible.

C. Luminosity

The quantity that measures the ability of a particle accelerator to produce the required number of interactions is the *luminosity*. It represents the proportionality factor between the number of produced events per unit of time, dR/dt, and the production cross-section of the considered reaction, σ_c:

$$\frac{dR}{dt} = \sigma_c \mathcal{L}. \tag{15}$$

In the specific case of a circular collider and when the particle density distribution can be approximated to a Gaussian, the luminosity of two beams, colliding exactly head-on, is given by:

$$\mathcal{L} = \frac{N_{b1}N_{b2}f_{\rm rev}k_b}{2\pi\sqrt{\sigma_{x1}^2 + \sigma_{x2}^2}\sqrt{\sigma_{y1}^2 + \sigma_{y2}^2}} = \frac{N_b^2 f_{\rm rev}k_b\gamma}{4\pi\epsilon_n\beta^*}, \tag{16}$$

where N_{b1} and N_{b2} are the two colliding bunch intensities, k_b the number of colliding bunches per beam, σ_{xi} and σ_{yi} are the transverse beam-sizes in the horizontal and vertical direction, respectively. The second equality follows in the approximation of equal and round distributions and optics of both beams: $N_b = N_{b1} = N_{b2}$, $\sigma_{xy} = \sigma_{xi} = \sigma_{yi} = \sqrt{\epsilon_n\beta^*/\gamma}$. With ϵ_n as the normalized emittance and β^* as the β-function at the interaction point (IP).

Using Table I and Eq. (16) the initial luminosity at the beginning of collisions computes to

$$\mathcal{L}_{\rm initial} = 2.6 \times 10^{27} \text{ cm}^{-2}\,\text{s}^{-1},$$

which is, due to the higher intensity and energy, already 2.6 times higher than the design luminosity for Pb-Pb of the LHC [8].

The total event cross-section, $\sigma_{c,\rm tot}$, is given by the sum over the cross-sections of all possible interactions removing particles from the beam in collision (burn-off). Apart from the inelastic hadronic interactions, the effects of bound free pair production (BFPP) and electromagnetic dissociation (EMD) are very important for Pb-Pb collisions:

$$\sigma_{c,\rm tot} = \sigma_{c,\rm BFPP} + \sigma_{c,\rm EMD} + \sigma_{c,\rm hadron}$$
$$\approx 354 \text{ b} + 235 \text{ b} + 8 \text{ b} = 597 \text{ b}. \tag{17}$$

The numerical values in Eq. (17) are estimated for $E_b = 50Z$ TeV with the aid of Refs. [21,22].

1. Luminosity evolution

While the beams are in collision, the instantaneous value of the luminosity will change, through intensity losses and emittance variations,

$$\mathcal{L}(t) = A\frac{N_b^2(t)}{\sqrt{\epsilon_x(t)\epsilon_y(t)}}, \tag{18}$$

where all time independent factors are merged in $A = f_{\rm rev}k_b/(4\,\pi\beta^*)$. For simplification, equal beam populations and sizes of both beams are assumed. To obtain the beam evolution with time, a system of four differential equations for the intensity, emittances and bunch length evolution has to be solved [23]. The solutions can be inserted into Eq. (18) to obtain the luminosity evolution.

$$\frac{dN_b}{dt} = -\sigma_{c,\rm tot}A\frac{N_b^2}{\sqrt{\epsilon_x\epsilon_y}}, \tag{19}$$

$$\frac{d\epsilon_x}{dt} = \epsilon_x(\alpha_{\rm IBS,x} - \alpha_{\rm rad,x}), \tag{20}$$

$$\frac{d\epsilon_y}{dt} = \epsilon_y(\alpha_{\rm IBS,y} - \alpha_{\rm rad,y}), \tag{21}$$

$$\frac{d\sigma_s}{dt} = \frac{1}{2}\sigma_s(\alpha_{\rm IBS,s} - \alpha_{\rm rad,s}). \tag{22}$$

The factor $1/2$ in Eq. (22) was introduced because the emittance growth rates are twice the amplitude growth rates. The change in particle number with time, dN_b/dt, is linked to the luminosity production rate described in Eq. (15). Now, $\sigma_c = \sigma_{c,\rm tot}$ is the sum of cross-sections for all processes that remove particles. A minus sign is introduced, since for each collision event generated one particle is lost: $dR/dt = -dN_b/dt$. The time evolution of the emittances and bunch length is influenced by dynamic

IBS growth and constant radiation damping. The total emittance growth rate $\alpha_\epsilon = \alpha_{\text{IBS}} - \alpha_{\text{rad}}$, thus varies dynamically in time and it is impossible to find an analytic solution of this system.

In the given form, Eq. (19) assumes that all beam losses are from luminosity burn-off. In LHC p-p operation, a large fraction of particles is lost on the collimators. The amount, however, strongly depends on the collimator settings, which in past runs (2012) were tight in order to clean the beam halo. Nevertheless, experience from RHIC shows that, owing to the applied stochastic cooling, it is possible to achieve very low loss rates from nonluminous processes [24]. The strong radiation damping at FCC energies will have a similar effect as the stochastic cooling in RHIC, supporting the assumption of negligible nonluminous losses made in Eq. (19).

In the following, approximations will be made for which an analytic description is possible. To simplify the situation, round beams and fully coupled transverse motion is assumed, such $\epsilon(t) = \epsilon_x(t) = \epsilon_y(t)$ at all times, reducing the ordinary differential equation (ODE) system to three equations.

(i) In the first case, $\epsilon(t) = \epsilon_0 = $ const. should be considered, which is achieved when $\alpha_{\text{IBS}} - \alpha_{\text{rad}} = 0$ and thus $d\epsilon/dt = 0$. For zero crossing angle, the bunch length evolution is (in first order) decoupled from the luminosity. Equation (19) simplifies to

$$\frac{dN}{dt} = -\sigma_{c,\text{tot}} A \frac{N_b^2}{\epsilon_0}.$$

This can easily be solved for the intensity evolution and, in combination with Eq. (18), for the luminosity evolution with time:

$$N_b(t) = \frac{N_{b0}}{AN_{b0}\sigma_{c,\text{tot}}t/\epsilon_0 + 1}$$

$$\Rightarrow \mathcal{L}(t) = \mathcal{L}_0 \left(\frac{1}{AN_{b0}\sigma_{c,\text{tot}}t/\epsilon_0 + 1}\right)^2.$$

By investigating those equations, it becomes clear that the only nonconstant factor is the time t, which appears only in the denominator, i.e., the intensity and with it the luminosity can only decay.

(ii) In the second case, the total emittance damping rate should be constant, $\alpha_\epsilon = $ const, with $\alpha_{\text{IBS}} \ll \alpha_{\text{rad}}$. It is implicitly approximated that IBS is independent of the beam parameters, decoupling the bunch length and emittance evolutions. Simultaneously solving the two remaining differential equations (19) and (20) gives

$$\epsilon_n(t) = \epsilon_0 \exp[-\alpha_\epsilon t] \qquad (23)$$

$$N_b(t) = \frac{N_{b0}\epsilon_0}{\epsilon_0 + AN_{b0}\sigma_{c,\text{tot}}(\exp[\alpha_\epsilon t] - 1)/\alpha_\epsilon} \qquad (24)$$

$$\mathcal{L}(t) = \mathcal{L}_0 \frac{\epsilon_0^2 \exp[\alpha_\epsilon t]}{[\epsilon_0 + AN_{b0}\sigma_{c,\text{tot}}(\exp[\alpha_\epsilon t] - 1)/\alpha_\epsilon]^2}. \qquad (25)$$

Again t is the only nonconstant parameter. As expected, $\epsilon_n(t)$ [Eq. (23)] and $N_b(t)$ [Eq. (24)] can only decay. However, the combination of both, the luminosity evolution [Eq. (25)], features the exponentially growing factor $\exp[\alpha_\epsilon t]$ in the numerator and denominator. This means, as long as the numerator $\epsilon_0^2 \exp[\alpha_\epsilon t]$ predominates the denominator $[\epsilon_0 + AN_{b0}\sigma_{c,\text{tot}}(\exp[\alpha_\epsilon t] - 1)/\alpha_\epsilon]^2$ a growth of the initial luminosity to a higher peak is possible. It should be noted that the assumption of a constant damping leads to emittances asymptotically approaching zero, which is nonphysical. Because of this effect, the luminosity peak computed with Eq. (25) is overestimated.

(iii) In reality the IBS growth rate changes dynamically with the intensity and emittance, thus it will become stronger, while the emittances shrink due to radiation damping. Since the total emittance growth rate is given by $\alpha_\epsilon = \alpha_{\text{IBS}} - \alpha_{\text{rad}}$, the emittance will approach a value where the growth from IBS balances the damping. This balance is not a real equilibrium, where the emittance and bunch length would be constant. But the IBS strength keeps decreasing due to intensity burn-off, leading to a slowly shrinking emittance and bunch length to maintain the balance.

An analytical expression for the balance value of the emittance and bunch length can be derived from Wei's IBS formalism given by Eq. (12) and (13). Even in this simplified form, the transverse growth rate shows a rather complicated dependence on ϵ, providing only a numerical solution. Both factors under the square root in the denominator of Eq. (12) depend on evolving beam properties. $\epsilon \propto 10^{-6}/\gamma \approx 10^{-11}$ and $C_2\sigma_p^2 \approx D_x^2/\beta_x(10^{-4})^2 \propto 10^{-10}$ are in the same order of magnitude, therefore we approximate $\sqrt{\epsilon + C_2\sigma_p^2} \rightarrow \sqrt{2C_2\sigma_p^2}$. Equation (12) can be set equal to $\alpha_{\text{rad},x}$ to satisfy the balance condition and be solved for the emittance $\epsilon_B = \epsilon_{n,B}/\gamma$:

$$\epsilon_{n,B} \cong \gamma \sqrt{\frac{C_1 N_b}{\sqrt{2C_2}\alpha_{\text{rad},x} D_p \sigma_{s,B}^2}}. \qquad (26)$$

D_p is the proportionality factor between the momentum spread and the bunch length given by Eq. (7). $\epsilon_{n,B}$ still depends on the balance value of the bunch length, $\sigma_{s,B}$, which is determined by replacing $\epsilon \rightarrow \epsilon_{n,B}/\gamma$ in Eq. (13) and applying $\alpha_{\text{IBS},s} = \alpha_{\text{rad},s}$:

$$\sigma_{s,B} \cong \left[\frac{C_3\sqrt{C_1 N_b \alpha_{\text{rad},x}}}{D_p^{5/2}(2C_2)^{1/4}\alpha_{\text{rad},s}}\right]^{1/3} \propto N_b^{1/6}. \qquad (27)$$

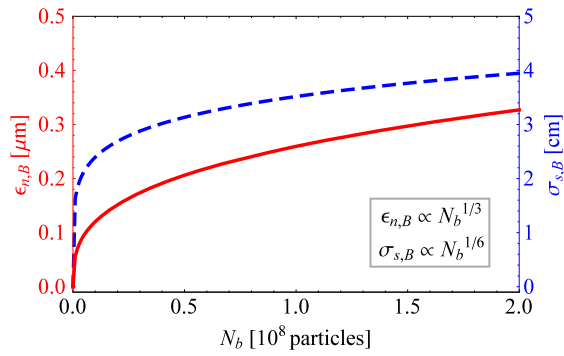Inserting Eq. (27) into Eq. (26) leads to an equivalent equation for the emittance:

FIG. 4.   Normalized emittance (red) and bunch length (blue) for balanced IBS and radiation damping.

$$\epsilon_{n,B} \cong \gamma \left(\frac{C_1 N_b D_p \alpha_{\mathrm{rad},s}}{C_3 \sqrt{2C_2} \alpha_{\mathrm{rad},x}^2} \right)^{1/3} \propto N_b^{1/3}. \qquad (28)$$

When a balance between IBS and radiation damping is reached, the emittance and bunch length depend only on the bunch intensity. The higher the number of particles, the larger the beam dimensions as shown in Fig. 4. The balanced normalized emittance (red) and the bunch length (blue) are plotted as a function of the intensity. The plot shows that those quantities become small in the expected range of bunch charge. Longitudinal, and potentially transverse, blow-up might become necessary to keep the beam sizes in a reasonable range.

The intensity evolution, where $\alpha_{\mathrm{IBS}} = \alpha_{\mathrm{rad}}$, can be obtained by inserting Eq. (28) into Eq. (19):

$$N_{b,B}(t) \cong 3\sqrt{3} N'_{b0}$$
$$\times \left(3 + 2^{5/6} A \sigma_{\mathrm{c,tot}} N'^{2/3}_{b0} t \left[\frac{C_3 \sqrt{C_2} \alpha_{\mathrm{rad},x}^2}{C_1 D_p \alpha_{\mathrm{rad},s}} \right]^{1/3} \right)^{-3/2}. \qquad (29)$$

Note that $N'_{b0} \neq N_{b0}$ is not the initial intensity at the beginning of the fill, but should be the number of particles left when the balanced regime is reached. The luminosity evolution can then be calculated by inserting Eq. (29) and (28) into (18).

Figure 5 shows the beam and luminosity evolution for case (ii) and (iii) as discussed above in comparison with tracking simulations done with the CTE program [3]. The results are displayed for two colliding lead bunches featuring the beam parameters given in Table I. One experiment is taking data. The black line shows the calculations with Eqs. (23)–(25) for the approximation where $\alpha_\epsilon = $ const. and $\alpha_{\mathrm{IBS}} \ll \alpha_{\mathrm{rad}}$. The dashed green line shows the calculations done with Eqs. (27)–(29) in the regime where IBS and radiation damping balance each other ($\alpha_{\mathrm{IBS}} = \alpha_{\mathrm{rad}}$). The two red lines are CTE simulations with (solid) and without (dashed) IBS coupling. The simulations are based on the assumption of a smooth lattice and Piwinski's IBS formalism.

It is clearly visible that the bunch length and emittances of the analytical calculations for $\alpha_{\mathrm{IBS}} \ll \alpha_{\mathrm{rad}}$ (black) asymptotically approach zero, which is nonphysical, leading to a strong overestimation of the luminosity. While the simulation with uncoupled planes (dashed red line) shows a realistic horizontal and longitudinal behavior, the vertical emittance still damps to zero. In the coupled simulation (solid red lines) all three beam dimensions settle at a balanced value above zero. The transverse normalized emittance reaches around 0.2 μm, corresponding to a beam size of $\sigma^* \approx 3$ μm at the IP for $\beta^* = 1.1$ m. The bunch length damps twice as fast as the transverse planes, before IBS kicks in and stabilises the bunch length around $\sigma_s \approx 3$ cm. The derivation of the balanced state equations (green dashed) assumes as well coupled transverse motion. The calculation is in very good agreement with the corresponding simulation.

Because of the small beam sizes, problems with instabilities might appear, apart from the fact that it could become difficult to find the collisions. Blow-up might become necessary in the longitudinal but maybe also in the transverse planes. A transverse emittance blow-up could also act as a luminosity leveling method.

Without further approximations it is not possible to solve the differential equation system of Eqs. (19)–(22) analytically. But by using Wei's analytic IBS expressions the system can be solved numerically. Figure 6 presents numerical solutions of the ODE system (dashed lines) obtained with *Mathematica*. Coupled transverse motion and round beams are assumed. The solid red line indicates again the CTE simulation shown in Fig. 5. The black dashed line shows the corresponding solution of the ODE system. The agreement between the numerical solution and the tracking result is excellent. Hence, the analytic calculation in the balanced regime (with coupling) is in excellent agreement with the ODEs. The small differences, are explained by the difference in IBS growth rates calculated with Piwinski's and Wei's algorithms for the same beam conditions. To prevent the bunch length from shrinking to too low values and to model the evolution under longitudinal blow-up, the ODEs are solved for constant bunch length ($d\sigma_s/dt = 0$, green dashed line). This enhances the intensity burn-off and the luminosity peak, since the IBS is weakened, reducing further the balance value of the emittance. Introducing an additional constant term in Eq. (20) can constrain the emittance above a certain value, $\epsilon_{\min}$, similar to the equilibrium between radiation damping and quantum excitation in lepton machines [6]:

$$\frac{d\epsilon}{dt} = \alpha_{\mathrm{IBS},x} \epsilon - \alpha_{\mathrm{rad}}(\epsilon - \epsilon_{\min}).$$

Solving the equations for both, constant bunch length and a minimum emittance of, e.g., $\epsilon_{\min} = 0.5$ μm, results in the blue dashed-dotted curve. As intended, the emittance stops

MICHAELA SCHAUMANN

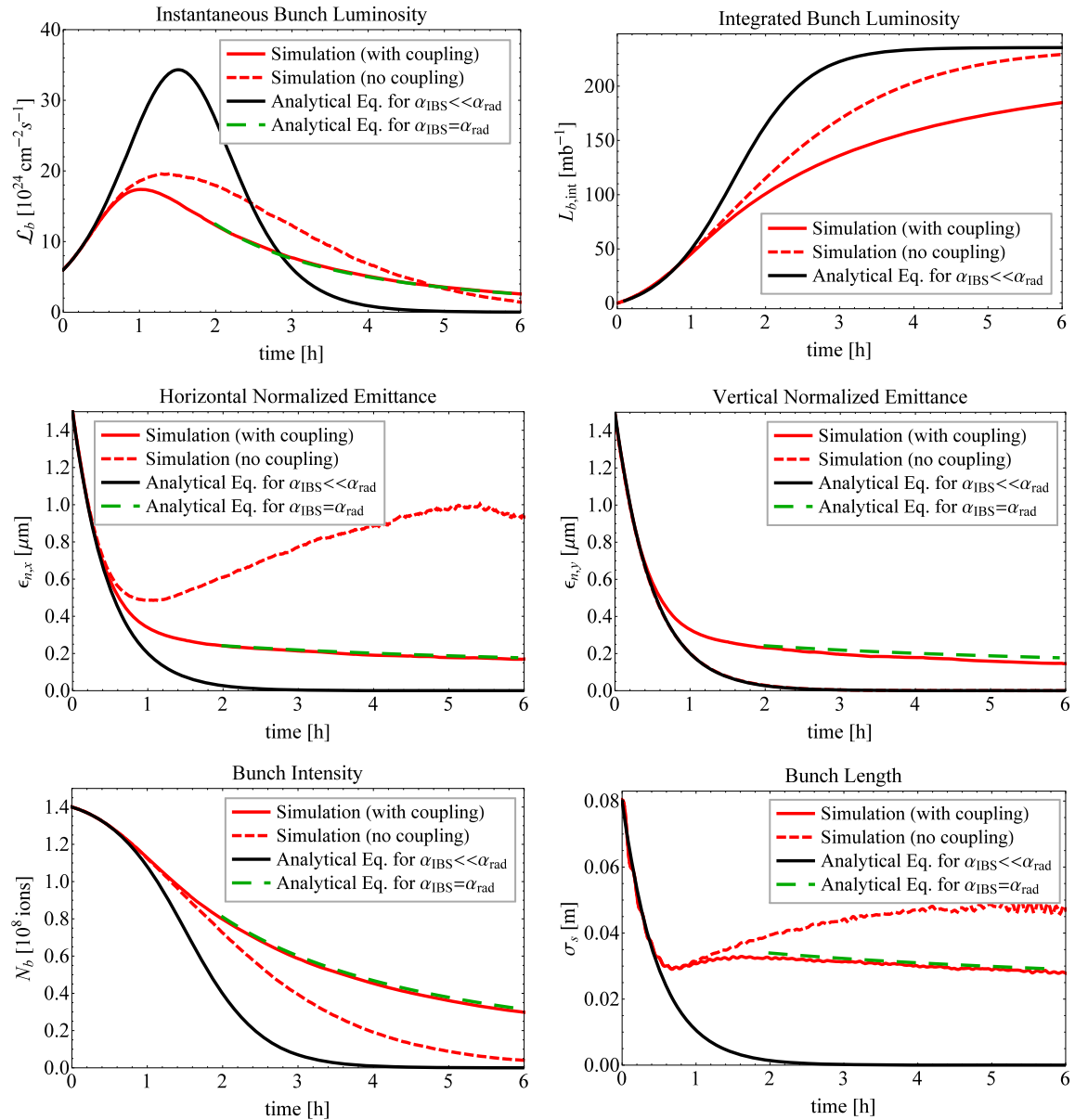Phys. Rev. ST Accel. Beams **18,** 091002 (2015)

FIG. 5. Pb-Pb beam and luminosity evolution. Top: instantaneous (left) and integrated luminosity (right), middle: horizontal (left) and vertical (right) normalized emittance, bottom: intensity (left) and bunch length (right). One experiment is in collisions. The black lines show the calculations done with Eqs. (23)–(25) for $\alpha_{IBS} \ll \alpha_{rad}$, the dashed green lines show the calculations done with Eqs. (27)–(29) in the regime where IBS and radiation damping balance each other ($\alpha_{IBS} = \alpha_{rad}$), the two red lines are CTE simulations with (solid) and without (dashed) IBS coupling. Note that the dashed red line in the middle right plot is hidden behind the black line.

decaying at about 0.5 μm, naturally coming along with a luminosity reduction.

Looking back at Fig. 5, the intensity decay is very fast, because of the high burn-off rates going along with the small emittances. In the analytical case (black) the total beam intensity is converted into luminosity in about 4 h. In the simulation the finite emittances reduce the peak luminosity and spread out the luminosity events over a longer period, however, the event production is still very efficient: only about 20% of the initial particles are left after 6 h collision time.

For comparison, in a normal LHC fill, the natural cooling from radiation damping is much weaker and not sufficient to increase the luminosity above its initial value. After about 6 h, the luminosity has decayed so much that it is necessary to refill. At that time, the beam population has only decreased to 40 or 50% of its initial value. Those particles have to be thrown away to be replaced with fresh beam. To maximize the integrated luminosity, the time in collisions has to be optimized.

In a very high energy hadron collider, the event production efficiency will be close to its optimum, where all
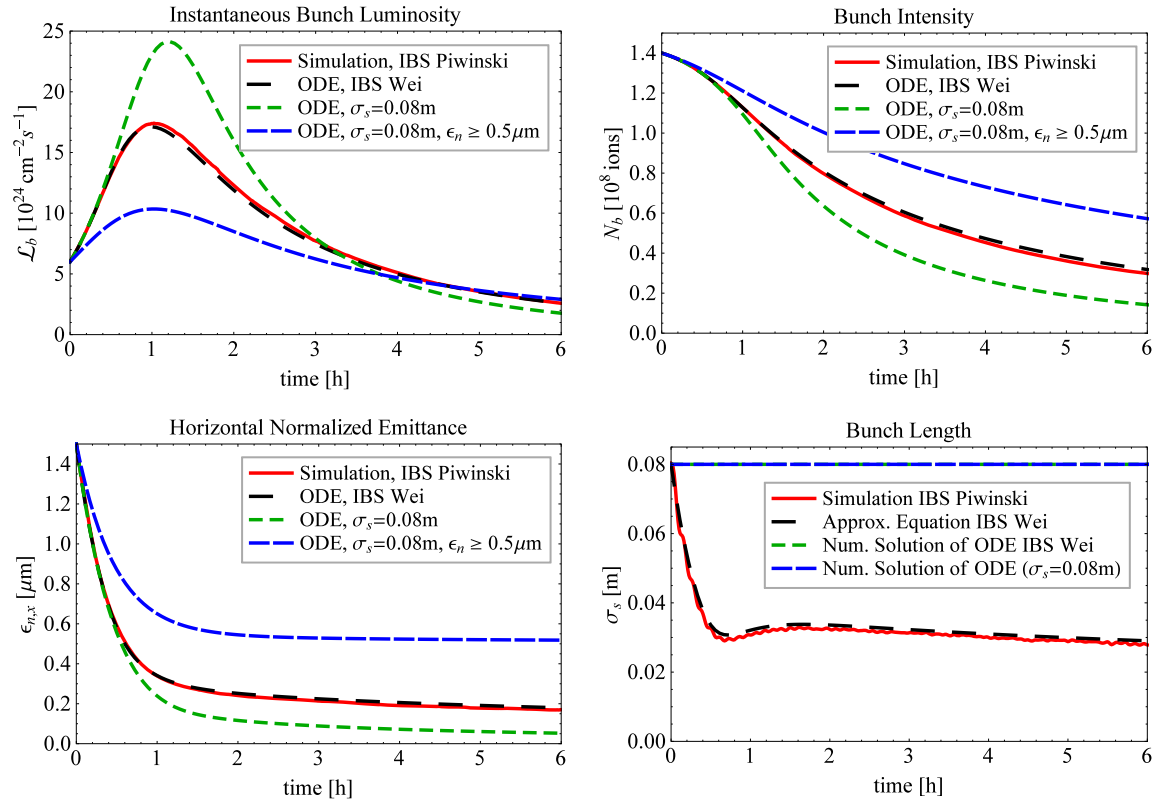
FIG. 6.   Pb-Pb beam evolution derived from ODE in comparison with simulation result. Top: Luminosity (left) and intensity (right), bottom: normalized emittance (left) and bunch length (right).

particles are converted into luminosity. Under equal operational conditions, this will lead to a constant fill length. In this regime the integrated luminosity per fill is given by

$$L_{int} = \frac{N_b k_b}{\sigma_{c,tot}}. \tag{30}$$

The simulations show that the luminosity evolution is not symmetric to the maximum, but it drops rather slowly once the balanced regime is reached. Depending on the turnaround time, t_{ta}, it is advantageous to dump the beams before all particles are burned-off and refill. The turnaround time is the time required to go back into collision after a beam abort. The average integrated luminosity defined as [4,25]

$$\langle L_{int} \rangle = \frac{1}{t_{coll} + t_{ta}} \int_0^{t_{coll}} L_{int}(t) dt \tag{31}$$

can be used to estimate the luminosity outcome per hour, depending on the expected turnaround time and time in collision, t_{coll}. In fact, for a given t_{ta} this equation can be used to find the duration t_{coll} for which $\langle L_{int} \rangle$ is maximized. Figure 7a shows $\langle L_{int} \rangle$/h as a function of t_{coll}. For $t_{ta} = 2$ h the maximum is reached after around $t_{coll} = 3$ h, which is about the time when the luminosity has decreased back to

its initial value. Under optimal running conditions, without failures and early beam aborts, from this point on it is more efficient to dump and refill, rather than collecting at low rates. As Fig. 7c displays, around 8 nb^{-1} (red solid line) could be collected during such an idealized 30 days Pb-Pb run. It is assumed that only one injection with two beams of 432 bunches each is taken from the LHC.

In general, a maximum of four injections would fit into the FCC. The total turnaround time consists of two components,

$$t_{ta} = t_{ta,FCC} + (n_{inj} - 1) t_{ta,LHC}$$

first $t_{ta,FCC}$, including everything done in the FCC (cycling to go back to injection energy, ramp, preparing collisions, etc.), and second $t_{ta,LHC}$, being the time between injections. n_{inj} is the number of LHC injections. The current LHC turnaround time is on average about $t_{ta,LHC} = 3$ h. Consequently, the already injected bunches would have to wait many hours at the FCC injection plateau. Simulations show that at this energy the Pb bunches lose about $R_{loss} = 5\%$ of their intensity per hour from debunching by IBS. For more intense bunches, the loss rate is enhanced. Approximating the intensity loss at the injection plateau as linear and neglecting losses during $t_{ta,FCC}$, the total colliding beam intensity can be estimated with

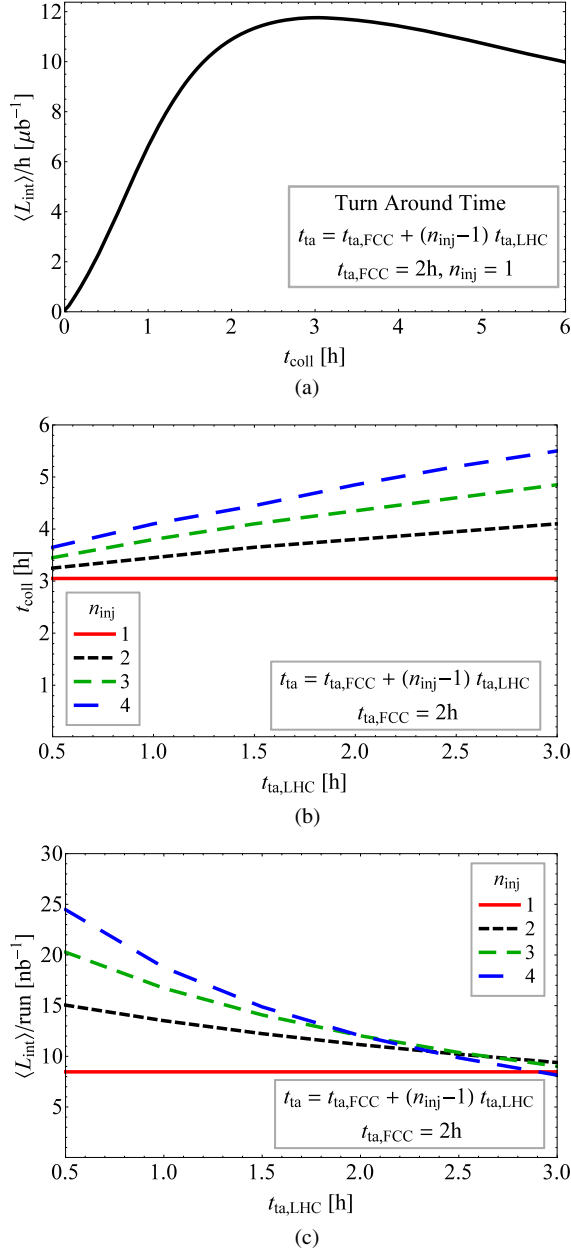MICHAELA SCHAUMANN

Phys. Rev. ST Accel. Beams **18**, 091002 (2015)

FIG. 7. (a) Average integrated luminosity per hour, (b) optimal time in collision, assuming different number of LHC injections, n_{inj}, (c) optimized integrated luminosity in a 30 days Pb-Pb run.

$$N_{beam} = k_b N_b \sum_{i=1}^{n_{inj}} [1 - R_{loss} t_{ta}(i-1)].$$

Dividing this by the injected beam intensity, $n_{inj} k_b N_b$, gives the fractional part of the intensity surviving until collision. Taking into account that $\mathcal{L} \propto N^2$, one can approximate that the potential luminosity is reduced by a factor $(N_{beam}/n_{inj} k_b N_b)^2$ due to IBS at the injection plateau.

Multiplying $\langle L_{int} \rangle$ by this factor leads to the estimates of $\langle L_{int} \rangle$/run shown in Fig. 7c for up to $n_{inj} = 4$. The corresponding optimal time in collision is displayed in

TABLE IV. Pb-Pb luminosity. The maximum integrated luminosity per bunch calculated with Eq. (30) is $L_{int,fill} = 0.235 \ \mu b^{-1}$.

	Unit	Per Bunch	k_b Bunches
$\mathcal{L}_{initial}$	[Hz/mb]	0.006	2.6
$\mathcal{L}_{peak}$	[Hz/mb]	0.017	7.5
$L_{int,fill}$	[μb^{-1}]	0.14	58.7
$L_{int,run}$	[nb^{-1}]	0.02	8.5

Fig. 7b. The total luminosity per run is shown as a function of the LHC turnaround time. This in an essential quantity to be improved for FCC, as it significantly influences the operation strategy. $t_{ta,FCC} = 2$ h is assumed. The plot makes clear, that the longer $t_{ta,LHC}$ the less attractive it becomes to inject more than once. It has to be considered that the larger n_{inj}, the higher the risk of losing an LHC fill during the injection process. This would lengthen the injection plateau by several hours and hence reduce the achievable luminosity. Moreover, for shorter $t_{ta,FCC}$, the crossing point of the curves shifts to the left, meaning that even for faster LHC cycles the potential luminosity outcome might be higher for fewer injections per fill. The unknown turnaround time imposes a large uncertainty on the estimates of $\langle L_{int} \rangle$ per hour and run. Any operational problems leading to delays will reduce the overall efficiency and reduce the estimated performance.

Table IV collects the numerical values for the initial, peak, and integrated luminosity per fill in Pb-Pb operation. The values quoted are taken from the simulation including coupling, to treat the most realistic case. The optimization is taken into account and the values are given for $n_{inj} = 1$, $t_{coll} = 3$ h, $t_{ta} = 2$ h and $t_{run} = 30$ days. The initial luminosity value is already 2.6 times over the nominal LHC, the peak could go up to around 7 times nominal LHC, which would be of the order of the requested LHC Pb-Pb luminosity for Run 3.

2. Luminosity lifetime

The luminosity lifetime is usually defined as the time at which the luminosity has decreased to $1/e$ of its initial value. Because of the radiation damping the luminosity evolution in the FCC does not follow an exponential decay and a new definition of the lifetime is to be agreed on.

Nevertheless, it should be mentioned, that in case of two exactly opposite experiments, taking data under the same conditions as discussed above, the luminosity lifetime will decrease accordingly, since the particle losses per turn are doubled.

D. Beam-beam tune shift

The two beams travel in separated beam pipes. Only in the interaction regions they do pass through a common pipe to bring them into collisions in the local experiment. In those regions of interaction the beams exert electromagnetic forces

on each other, the so-called beam-beam force. Especially during the passage of one bunch through the other in the IP, during a so-called *head-on* interaction, those forces can be very strong. In a simplified picture, each single particle of one bunch receives a kick from the opposite beam and is deflected by a certain angle. In a linear approximation this kick acts as a quadrupole lens and thus introduces a tune shift, which can be approximated with the linear beam-beam parameter ξ [6]:

$$\xi_{i,u} = \frac{N_{b,j} r_{p0} Z_i Z_j \beta^*}{2 \pi A_{\text{ion},i} \gamma_i \sigma_{j,u} (\sigma_{j,u} + \sigma_{j,v})}, \qquad (32)$$

where the beam receiving the kick is labeled with i and the beam exerting the force is labeled j. u and v describe the two transverse planes. r_{p0} is the classical proton radius, Z and A_{ion} the charge and atomic mass number of the corresponding beams, σ the beam size in the corresponding plane.

For equal and round beams Eq. (32) simplifies to

$$\xi = \frac{N_b r_0 \beta^*}{4 \pi \gamma \sigma^2} = \frac{N_b r_0}{4 \pi \epsilon_n} = 3.7 \times 10^{-4}, \qquad (33)$$

with r_0 as the classical radius of the considered particle and ϵ_n the normalized emittance. As it is easy to see, this equation only depends on the beams themselves and is independent of energy and lattice parameters. Equations (32) and (33) describe the tune shift introduced due to one head-on collision per turn, if the beams collide in more than one place, ξ has to be multiplied by the number of experiments in which the investigated bunch is colliding. The numeric value in Eq. (33) was obtained with the initial parameters given in Table I.

The beam-beam tune shift can be a limiting factor for the luminosity, since, if it becomes too large, the particles could cross resonances and get lost. If this is the case, the intensities have to be reduced or the emittances blown-up to force the tune shift below its limit, consequently the luminosity will be reduced simultaneously. N_b and ϵ_n change during the fill and thus the beam-beam tune shift. This is especially important in the case discussed here, since with the damped emittance, the tune shift increases. From the simulation results displayed in Fig. 5 the intensity and emittance evolutions are combined to determine the variation of the beam-beam tune shift during a fill with one experiment in collisions, see Fig. 8.

The peak value reaches $\xi \approx 1.4 \times 10^{-3}$. If more than one experiment is taking data, this tune shift should be multiplied by the number of experiments. However, this is not exactly true for the curve in Fig. 8, since it was obtained from the simulated beam evolution considering one active IP. The curve would change slightly (to lower values), due to the faster intensity burn-off and thus the beam evolution for two or more experiments would be different.
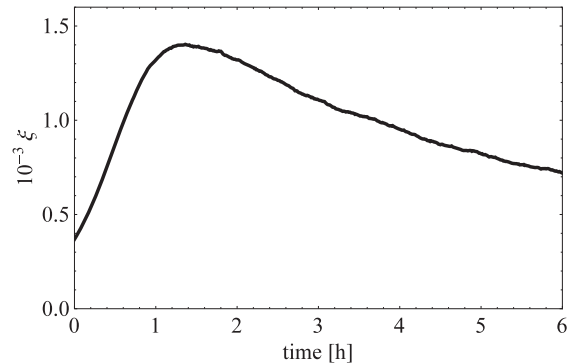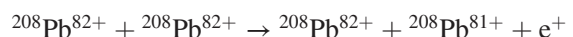

FIG. 8. Evolution of the beam-beam tune shift for one experiment in collision.

Only during operation does it become certain where the beam-beam limit of a collider exactly is. For the *p-p* operation in the LHC, for instance, a beam-beam limit of 0.015 was expected, based on the Sp$\bar{\text{p}}$S experience. Nevertheless, the tune shifts achieved in *p-p* in dedicated experiments exceeded the nominal value by almost a factor of 5 and the value reached in normal operation by already a factor of 2 [26].
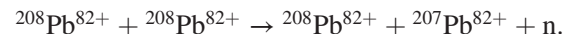
Comparing to those factors, and taking into account that the usual tune stability in the LHC is in the order of 10^{-3}, the beam-beam tune shift in Pb-Pb operation for FCC is not negligible, but probably also not at the limit.

E. Bound-free pair production power

Ultraperipheral electromagnetic interactions dominate the total cross-section during heavy-ion collisions, see Eq. (17), and cause the initial intensity to decay rapidly [27]. The most important interactions in Pb collisions are bound-free pair production (BFPP)

$$^{208}\text{Pb}^{82+} + \,^{208}\text{Pb}^{82+} \rightarrow \,^{208}\text{Pb}^{82+} + \,^{208}\text{Pb}^{81+} + \text{e}^+$$

and electromagnetic dissociation (EMD)

$$^{208}\text{Pb}^{82+} + \,^{208}\text{Pb}^{82+} \rightarrow \,^{208}\text{Pb}^{82+} + \,^{207}\text{Pb}^{82+} + \text{n}.$$

The above equations only describe the first order reactions. In higher order reactions two or more electrons are captured or neutrons are emitted, but those occur with reduced interaction cross-sections compared to the first order processes. These interactions change the charge state or mass of one of the colliding ions, creating a secondary beam emerging from the collision point. The resulting momentum deviation of the secondary beam lies outside the momentum acceptance of the ring, resulting in an impact on the beam screen in a localized position (depending on the lattice) most probably around a superconducting magnet downstream the IP. This occurs on each side of every IP where ions collide.

MICHAELA SCHAUMANN

Phys. Rev. ST Accel. Beams **18**, 091002 (2015)

Following Eq. (15), the production rate of those processes is proportional to the instantaneous luminosity and will thus change during the fill. Nevertheless, the magnets would suffer from a continuous high exposure. Already under LHC conditions, the risk of quenching a superconducting magnet due to these losses is high [28]. In the FCC the peak luminosity could be an order of magnitude higher, increasing the risk even further. The power, P, in those secondary beams can be calculated as the production rate times the particle energy:

$$P = \sigma_c \mathcal{L} \gamma m_{\text{ion}} c^2.$$

Figure 9 shows the power evolution of the BFPP1 beam (^{208}Pb^{81+} ions, capture of one e^-), which has the highest cross-section and accordingly the highest intensity and damage potential. For the calculation the total BFPP cross-section, $\sigma_{\text{BFPP}} = 354$ b at $50Z$ TeV, estimated with [21], was used. The probability of higher order interactions, i.e., capturing two or more electrons and leading to a charge state of $\leq 80^+$ is much smaller and ignored for the purpose of estimating the upper limit of the power carried by the most intense secondary beam.

For the computation of the beam power, the simulated luminosity, shown in Fig. 5, was used. The maximum power goes up to $P \approx 1.7$ kW, but already the initial value of 606 W would lead to quenches and prevent from operating the machine. Depending on the aperture and optics in the FCC, the EMD1 beam (^{207}Pb^{82+} ions, emission of one neutron) might as well hit the beam screen, depositing additional energy. For comparison, the BFPP1 beam power in the nominal LHC is about 26 W, which is already expected to cause operational problems and, possibly, long-term damage. Countermeasures would definitely be required to absorb those particles before they can impact on the superconducting magnets. It has to be studied, if a highly resistant collimator in the dispersion suppressor region, as discussed for HL-LHC heavy-ion operation [29,30], would be sufficient to stop the beams produced in the collisions at the highest energy of the FCC.
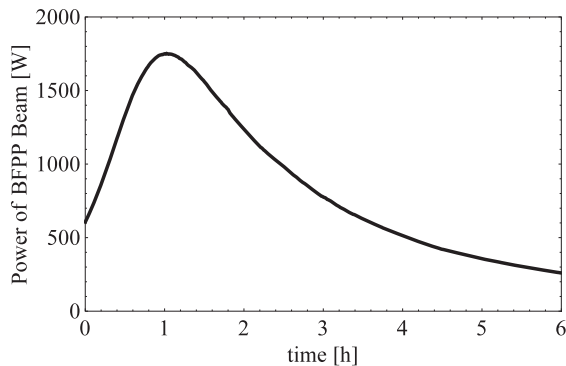

FIG. 9. BFPP1 beam (^{208}Pb^{81+} ions) power evolution in Pb-Pb operation.

IV. PROTON-LEAD OPERATION

A. Beam and luminosity evolution

IBS approximately scales with $r_0^2 \propto (Z^2/A_{\text{ion}})^2$ and is therefore weaker for protons than for lead ions. In fact, IBS is negligible for the (initial) proton beam parameters used in p-Pb operation at top energy. The radiation damping rates in Eq. (14) show a dependence on the particle type as $(E_b Z)^3 r_0 / m_{\text{ion}}^3 \propto Z^5 / A_{\text{ion}}^4$. Calculating this ratio shows that the radiation damping for lead is about twice as fast as for protons at the same magnetic rigidity. Thus, the emittances of both beams evolve with different time constants. Consequently, eight differential equations, four per beam, have to be solved simultaneously to describe the beam and luminosity evolution for p-Pb collisions. Those could be reduced to six equations by assuming fully coupled transverse motion and round beams, in this case $\epsilon(t) = \epsilon_x(t) = \epsilon_y(t)$ holds at all times. Rewriting Eq. (16) under this approximation leads to the instantaneous luminosity for p-Pb

$$\mathcal{L} = A \frac{N_b(p) N_b(\text{Pb})}{\epsilon(p) + \epsilon(\text{Pb})}, \tag{34}$$

with $A = f_{\text{rev}} k_b / (2 \pi \beta^*)$. With this, the differential equation system follows

$$\frac{dN_b(\text{Pb})}{dt} = -\sigma_{c,\text{tot}} A \frac{N_b(p) N_b(\text{Pb})}{\epsilon(p) + \epsilon(\text{Pb})} \tag{35}$$

$$\frac{d\epsilon(\text{Pb})}{dt} = \epsilon(\text{Pb})[\alpha_{\text{IBS},x,y}(\text{Pb}) - \alpha_{\text{rad},x,y}(\text{Pb})] \tag{36}$$

$$\frac{d\sigma_s(\text{Pb})}{dt} = \frac{1}{2} \sigma_s(\text{Pb})[\alpha_{\text{IBS},s}(\text{Pb}) - \alpha_{\text{rad},s}(\text{Pb})], \tag{37}$$

where only the three equations of the Pb beam are noted. The equations for the proton beam have an equivalent form with different initial conditions and growth rates. The dependences of the IBS growth rates on N_b, ϵ and σ_s couple the three equations for each beam. The dependence of the luminosity on both beams' emittances and intensities couple the Pb and p beam evolution. An exact analytic solution of this coupled differential equation system does not exist. Unfortunately, the CTE program does not feature simulations with different particle species, so only approximated analytical and numerical solutions of the ODE system are available to perform estimates.

At the beginning of the fill, $\alpha_{\text{IBS}} \ll \alpha_{\text{rad}}$ and it can be approximated that $\alpha_\epsilon = \alpha_\epsilon(\text{Pb}) = 2\alpha_\epsilon(p) = $ const. in all three planes. This constant emittance decay rate, neglects the dynamically changing IBS with damped emittance. As seen in the Pb-Pb analysis, the peak and integrated luminosity estimates done under those assumptions will

be overestimated, due to the emittances asymptotically approaching zero.

In general, the proton beams are more intense compared to lead. In the LHC proton-proton operation, bunches with 10^{11} particles are regularly used. Lead bunches have in the order of 10^8 particles. In proton-lead operation, it is possible to increase the initial luminosity by increasing the proton intensity (the lead intensity is assumed to be at the limit). Nevertheless, the higher the proton intensity, the stronger the beam-beam effects in those strong-weak interactions. Therefore, it was chosen for the LHC proton-lead run in 2013 [11] to use proton intensities around 10% of the nominal value used in *p*-*p* operation. Based on the experiences from this first *p*-Pb run of the LHC, this should also be the baseline for *p*-Pb collision mode in FCC-hh.

In each collision of a proton with a lead ion, those two particles are removed from their beams. Therefore, the maximum integrated luminosity is reached when each lead ion has found a collision partner in the more intense proton beam. The number of lead ions is only about 1% of the number of protons. In the limit of burning-off all the lead, the proton intensity is hardly changed and could be considered as roughly constant through the whole fill.

To find an approximated analytical equation for the proton-lead luminosity evolution, the following assumptions are made:

$$N_b(\text{Pb}) \ll N_b(p) = N_{b0}(p) = \text{const}, \tag{38}$$

$$\alpha_\epsilon = \alpha_\epsilon(\text{Pb}) = 2\alpha_\epsilon(p) \approx -\alpha_{\text{rad}}(\text{Pb}), \tag{39}$$

$$\alpha_{\text{rad},s} = 2\alpha_{\text{rad},x,y}, \tag{40}$$

where Eq. (39) is assumed for all three planes and Eq. (40) follows from Eq. (14). Applying those constraints to the differential equations (35)–(37) leads to an exponential behavior of the emittance and bunch length of both beams with related time constants

$$\epsilon(\text{Pb}, t) = \epsilon_0(\text{Pb}) \exp[\alpha_\epsilon t], \tag{41}$$

$$\sigma_s(\text{Pb}, t) = \sigma_{s0}(\text{Pb}) \exp[\alpha_\epsilon t], \tag{42}$$

$$\epsilon(p, t) = \epsilon_0(p) \exp[\alpha_\epsilon t/2], \tag{43}$$

$$\sigma_s(p, t) = \sigma_{s0}(p) \exp[\alpha_\epsilon t/2], \tag{44}$$

where the emittance growth rate of the Pb beam is taken as the reference, $\alpha_\epsilon \approx -\alpha_{\text{rad},x,y}(\text{Pb})$. This value is negative, hence those are exponential decays. The proton intensity was assumed to be time independent, thus

$$N_b(p, t) = N_{b0}(p). \tag{45}$$

To solve the last equation for the Pb intensity evolution, Eqs. (41), (43), and (45) are inserted into Eq. (35), followed by applying the method of separation of variables. The solution of the arising integral is

$$\ln(N_b(\text{Pb}, t)) = \int \frac{\mathrm{d}x}{x^2(ax+b)} = -\frac{1}{bx} + \frac{a}{b^2}\ln\left(\frac{ax+b}{x}\right)$$

with $x = \exp[\alpha_\epsilon t/2]$. The final result is

$$N_b(\text{Pb}, t) = N_{\text{Pb}} e^{-\frac{2\sigma_{c,\text{tot}}AN_p}{\alpha_\epsilon \epsilon_p^2}(\epsilon_p(\exp[-\alpha_\epsilon t/2]-1)+\epsilon_{\text{Pb}}\ln[\epsilon_p+\epsilon_{\text{Pb}}]-\epsilon_{\text{Pb}}\ln[\epsilon_p \exp[-\alpha_\epsilon t/2]+\epsilon_{\text{Pb}}])}.$$

The equations for the evolution of the emittance and intensity are inserted into Eq. (34) to obtain the *p*-Pb luminosity evolution. Figure 10 presents the results. The above derived analytical approximation is shown as the solid lines, while the dashed lines correspond to the numerical solution of the ODE system. The evolution of the intensity (middle left), beam size at the IP (middle right), and bunch length (bottom) are displayed in black for the proton and in red for the lead beam.

The peak luminosity is shifted to later times compared to Pb-Pb operation, due to the slower radiation damping for protons, leading to longer fills. The Pb intensity burn-off is very fast, while the proton intensity hardly changes. This arises from the fact that in one collision one Pb nucleus is lost per proton. A free knob to adjust the luminosity peak and evolution is the proton intensity. Increasing $N_b(p)$ would lead to higher initial and peak rates followed by an even faster Pb burn-off and shorter fills. Decreasing $N_b(p)$ would distribute the

achievable luminosity over a longer period with reduced peak rates.

B. Optimizing the integrated luminosity

Because of the weaker IBS for protons, their intensity losses at injection are smaller and the proton beam can wait in the machine without deteriorating significantly. Therefore, the proton beam is injected first, followed by the lead. Depending on the number of injections, either both LHC rings are filled with the same species, or the filling is shared between the species and each LHC beam is injected in opposite directions in the FCC. In this way the number of particles surviving until top energy is maximized.

From the numerical solution of the ODE system, which provides the best estimate of the beam and luminosity evolution available today, the average luminosity per hour is determined. Similar to Pb-Pb, an expression for the total available *p* and Pb beam intensity in collision is derived, taking into account the different waiting times and
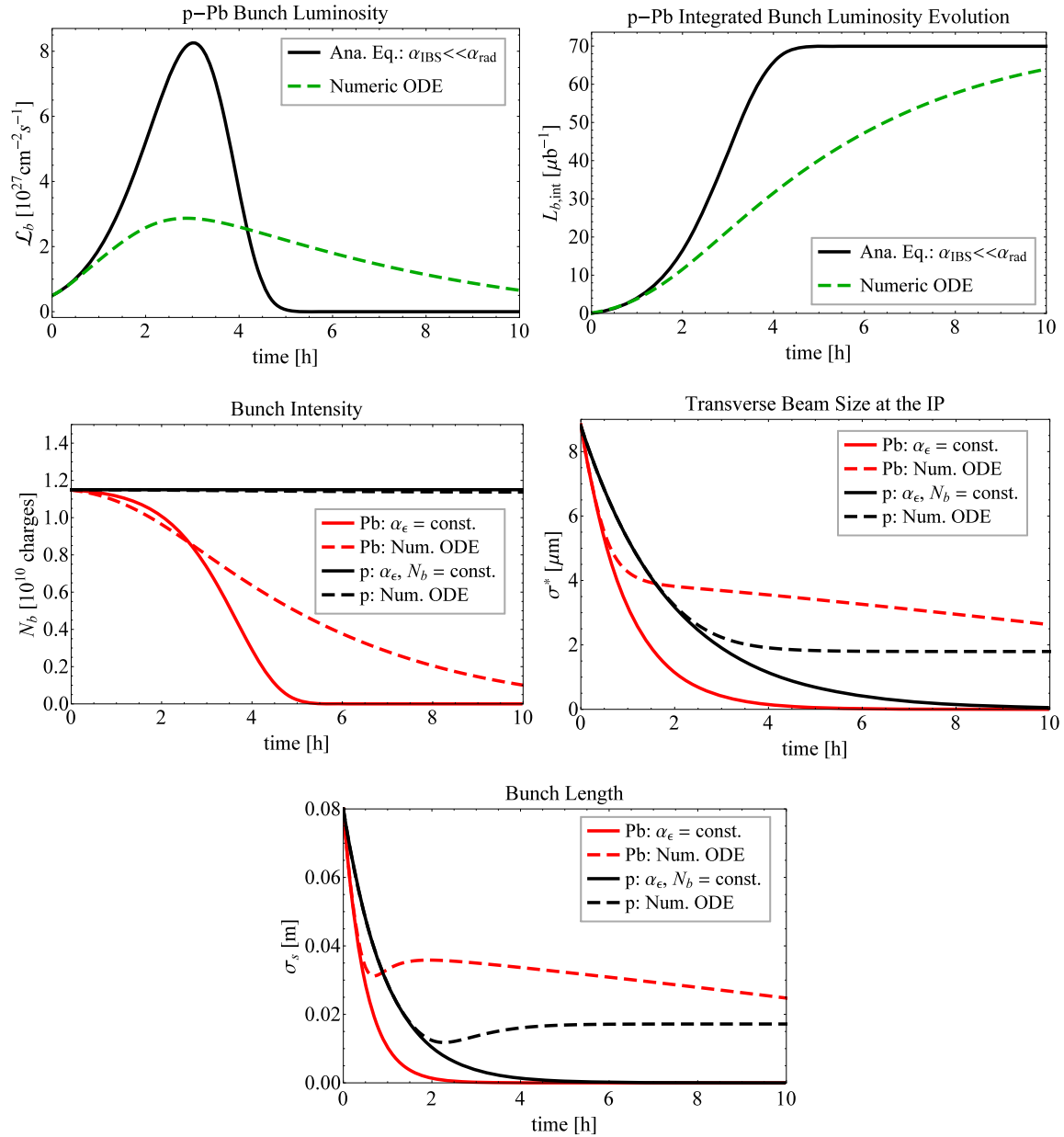
FIG. 10.   *p*-Pb beam and luminosity evolution for one experiment in collisions. Top: instantaneous (left) and integrated (right) bunch luminosity, middle: intensity (left) and beam size at the IP (right), bottom: bunch length for the proton (black) and lead (red) beam. Approximated analytic calculations (solid lines), neglect the dynamically changing IBS, leading to unrealistically small beam sizes. The numerical ODE solution is shown as dashed lines, giving more realistic estimates.

loss rates at the injection plateau. The average luminosity per hour is then calculated as in Eq. (31) reduced by the factor

$$[N_{\text{beam}}(\text{Pb})/n_{\text{inj}}k_b N_b(\text{Pb})] \times [N_{\text{beam}}(p)/n_{\text{inj}}k_b N_b(p)]$$

(46)

for losses during injection.

Figure 11 shows the results for the average integrated luminosity (a) and the corresponding time in collisions

(b) to achieve the optimized integrated luminosity per 30 days run (c). For $n_{\text{inj}} = 1$ the maximal luminosity of 1.8 pb^{-1}/run is reached for a fill length of 6.5 h. This does not take into account any delays or early aborted fills changing the assumed optimized statistics. Again it becomes clear that the longer the LHC turnaround time, the less attractive it becomes to wait for more injections before colliding. The collectable luminosity decreases, due to particle losses on the lengthened injection plateau. Moreover, the optimal fill length becomes longer,
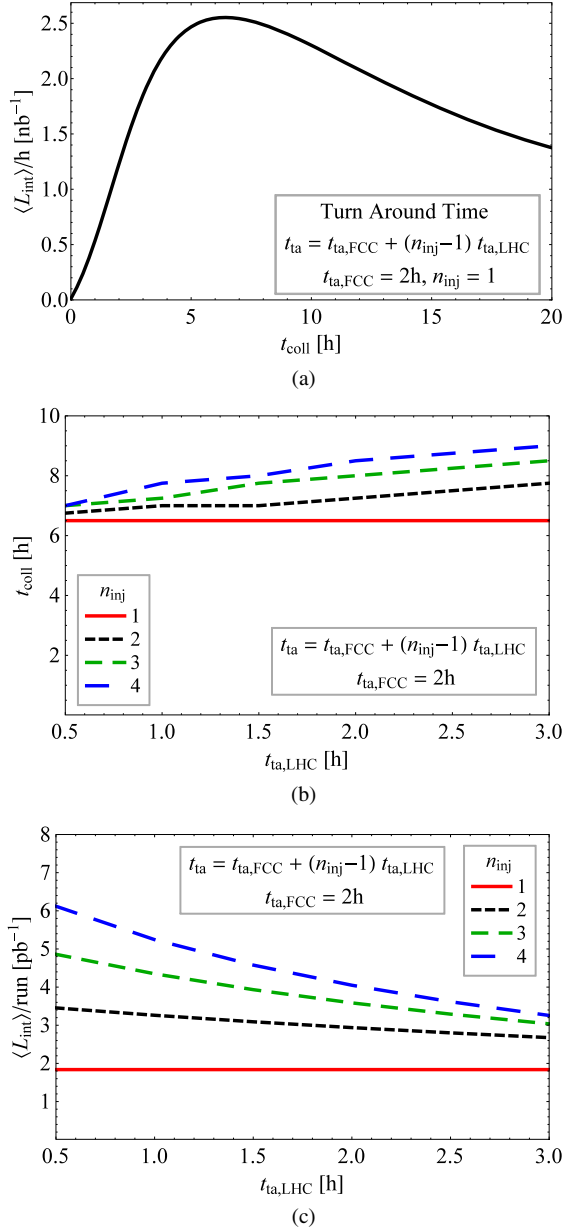
TABLE V. p-Pb luminosity. $\sigma_{c,\text{tot}} = 2$ b was used. The maximum integrated luminosity per fill calculated with Eq. (30) is $L_{\text{int}} = 30$ nb^{-1}.

	Unit	Per Bunch	k_b Bunches
$\mathcal{L}_{\text{initial}}$	[Hz/mb]	0.5	213
$\mathcal{L}_{\text{peak}}$	[Hz/mb]	2.9	1240
$L_{\text{int,fill}}$	[μb^{-1}]	50.1	21648
$L_{\text{int,run}}$	[nb^{-1}]	4.2	1837

Consequently, the ion beam lifetime determines the length of the fill in p-Pb operation.

The beam current lifetime is given by

$$\frac{1}{\tau_N} = -\frac{1}{N}\frac{dN}{dt} = -\frac{1}{N}\sigma_{c,\text{tot}}\mathcal{L},$$

with $N = k_b N_b$ and $N_b = N_b(\text{Pb})$. Inserting Eq. (34) for the luminosity, the Pb beam current lifetime in p-Pb collisions is

$$-\tau_N(\text{Pb},t) = \frac{2\,\pi\beta^*[\epsilon(p,t) + \epsilon(\text{Pb},t)]}{\sigma_{c,\text{tot}} n_{\text{exp}} f_{\text{rev}} N_b(p)}. \quad (47)$$

The first factor is constant for $N_b(p) \gg N_b(\text{Pb})$. Hence, the lifetime only varies in time proportionally to the convoluted emittance of the two beams. As expected, $\tau_N(\text{Pb})$ decreases with increasing proton intensity, because of the higher interaction probability. The initial value evaluates to

$$\tau_N(\text{Pb}, t = 0) = 39.3 \text{ h}$$

for $n_{\text{exp}} = 1$. Owing to the damping of the emittances, these values will decrease exponentially during the fill and lead to a much shorter fill duration. Note that Eq. (47) is independent of the lead beam current.

D. Beam-beam effects

1. Unequal beam sizes

The initial beam sizes of the proton and lead beam in p-Pb operation is assumed to be equal. Because of the stronger radiation damping for Pb, the Pb beam size falls below the proton beam size in the first period of the fill, see Fig. 10. After about one hour in collisions the Pb emittance reaches the balanced regime and does now change only slowly due to the intensity losses and the thus decreasing IBS rate. Since the IBS is weaker for protons, the emittance is damped to a lower value. After about 1.5 h in collisions the proton beam has become smaller than the Pb beam. Over the duration of the fill, the ratio of the Pb to the proton beam size lies between $0.8 \leq \sigma_{\text{Pb}}/\sigma_p \leq 1.9$.

FIG. 11. (a) Average integrated luminosity per hour, (b) optimal time in collision, (c) optimized integrated luminosity for a 30 days p-Pb run.

enhancing the risk to be aborted ahead of schedule, potentially decreasing the predicted luminosity further. Table V summarizes the initial, peak, and integrated luminosity values in p-Pb operation.

C. Beam current lifetime

As mentioned, the ion beam is naturally weak, while proton beams can be produced with much higher intensities. In the collision the lead beam loses $Z = 82$ charges per lost proton. Thus, the ion beam will in general have the smaller beam current lifetime, i.e., faster intensity decay.

From experience at various past colliders, it is well known that beam lifetime can be significantly reduced when colliding beams have unequal sizes [31–33]. It is observed that the lifetime of the larger beam decreases with decreasing size of the opposite beam. This is because the particles in the beam with the larger size see more of the nonlinear part of the beam-beam force exerted by the smaller beam, where they are affected by higher order resonances [32].

In case of the FCC p-Pb operation, the difference in beam size stays below 20% over the first two hours, including a reversal of the rank. For the latter part of the fill, the Pb beam is the larger and thus might suffer from a lifetime reduction. Considering the optimum fill length of 6.5 h and the evolution of the luminosity in Fig. 10, the largest fraction of the luminosity is integrated in the first four hours of the fill. Comparing this to the discussed evolution of $\sigma_{\text{Pb}}/\sigma_p$ indicates that a potential reduction of the Pb beam lifetime due to unequal beam sizes would probably affect the luminosity only in the second half of the fill, when the collision rates have already passed the maximum.

For comparison, the Tevatron ran with mismatched beam sizes between the proton and antiproton beam of around $\sigma_p/\sigma_{\bar{p}} \approx 3$ [34]. In the first p-Pb run of the LHC in 2013, $\sigma_{\text{Pb}}/\sigma_p \approx 2$ was observed, while the beam lifetime was dominated by other effects [11].

2. Tune shift

With Eq. (32) the beam-beam tune shift ξ can be calculated for weak-strong beam-beam interactions as in the case of p-Pb collisions. The initial beam parameters in Table I are such that the number of charges and the beam sizes of both beams are approximately equal, resulting in the same tune shift, $\xi(p) \approx \xi(\text{Pb}) = 3.7 \times 10^{-4}$, at the beginning of the fill. However, the proton and lead beam properties evolve differently with time, changing the force exerted from one to the other during the fill. Figure 12 shows the calculation of ξ based on the numerical solution of the ODE system. The effect on the proton (black) beam is small $[\xi(p) < 2 \times 10^{-3}]$. The increase of $\xi(p)$ due to the
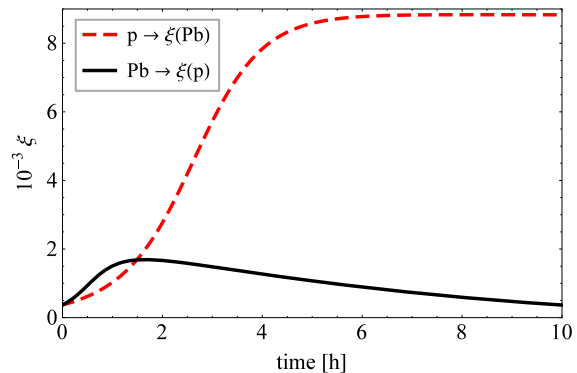

FIG. 12. p-Pb beam-beam tune shift for 1 IP in collision.

shrinking lead beam emittances is negated by the rapid Pb intensity losses. Owing to the almost constant proton intensity but damping emittances, the tune shift to the Pb beam becomes significant and approaches a value of $\xi(\text{Pb}) = 8.8 \times 10^{-3}$ in the regime where IBS and radiation damping start to balance each other. This value is close to the assumed beam-beam limit of $\xi = 0.01$ for p-p operation.

V. PROTON-PROTON OPERATION

In the following the tools used in the above analysis are applied to p-p operation in the FCC. In p-p operation two scenarios are under investigation, namely bunches spaced by 25 or 5 ns with different beam properties. The proton beam parameters are listed in Table VI.

Radiation damping is negligible for protons at injection energy. At 50 TeV the transverse and longitudinal emittance radiation damping times are $1/\alpha_{\text{rad},x,y} = 1.0$ h and $1/\alpha_{\text{rad},s} = 0.5$ h, respectively. The horizontal equilibrium emittance from quantum excitation at top energy is in the order of 10^{-2} μm, which is still an order of magnitude smaller than the emittance ranges of the scenarios considered.

As already explained, depending on the lattice choice, the IBS growth rates can be rather different. Figure 13 shows the IBS growth times as a function of the FODO

TABLE VI.   Assumed beam parameters for proton-proton operation [4].

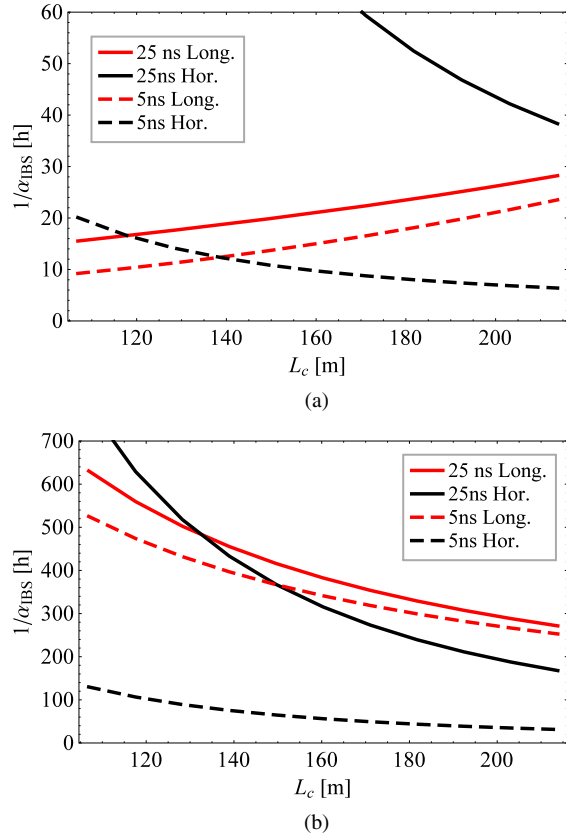| Parameter	Symbol	Unit	25 ns	5 ns
Number of particles per bunch	N_b	$[10^{11}]$	1.0	0.2
Normalized transverse emittance	ϵ_n	$[\mu$m$]$	2.2	0.44
rms bunch length	σ_s	[m]	0.08	0.08
Number of bunches per beam	k_b	$\cdots$	10600	53000
β-function at IP	β^*	[m]	1.1	1.1
Total cross section	$\sigma_{c,\text{tot}}$	[mb]	153	153
Number of main IPs	$\cdots$	$\cdots$	2	2

FIG. 13.   Initial IBS growth times and their dependence on the FODO cell length, L_c, at injection (a) and top energy (b) for p-p operation.

cell length, L_c, at (a) injection and (b) top energy. The same behavior as for Pb is observed, whereas the rates are lower. For the chosen baseline lattice with $L_c \approx 203$ m and $\gamma_T \approx 103$, the initial growth times calculated with Piwinski's algorithm are listed in Table VII. IBS is in general small for the initial proton beam parameters. Only the horizontal growth time at injection is below 10 h, which might lead to transverse emittance growth, if the time spent on the injection plateau becomes too long.

In Fig. 14 the luminosity and beam evolution in p-p operation is displayed. The solid lines show the free beam evolution without any artificial blow-up, obtained by solving an ODE system of the form (19)–(22) for two experiments in collision. The dashed lines represent the solution of the following differential equations:

$$\frac{\mathrm{d}N_b}{\mathrm{d}t} = -\sigma_{c,\text{tot}}A\frac{N_b^2}{\epsilon}$$

$$\frac{\mathrm{d}\epsilon}{\mathrm{d}t} = \alpha_{\text{IBS},x}\epsilon - \alpha_{\text{rad},x}\left(\epsilon - \frac{N_b}{N_{b0}}\epsilon_0\right)$$

$$\frac{\mathrm{d}\sigma_s}{\mathrm{d}t} = 0,$$

here a constant bunch length and a transverse emittance blow-up designed to keep the beam-beam parameter ξ at its initial value is implemented. For the FCC study it is assumed that the peak luminosity is limited by a maximum beam-beam tune shift of $\xi = 0.01$, from which the initial beam parameters were derived. Leaving the beams to evolve freely leads to an increase of up to ~5 times this value, as shown in the bottom right plot of Fig. 14. In this case, the bunch length shrinks to about 2 cm, which is most probably not acceptable for the experiments. The transverse normalized emittances balance around 0.2 μm. The peak luminosity reaches 16×10^{34} cm^{-2} s^{-2} for 25 ns and to 11×10^{34} cm^{-2} s^{-2} for the 5 ns scenario. Since the beam-beam parameter is proportional to N_b/ϵ, the luminosity will decay exponentially, if $\xi =$ const. This luminosity decay could be mitigated by β^*-leveling. The minimum β^* is constrained by the aperture in the triplet, thus β^* could be lowered proportionally to the shrinking emittance, resulting in an about constant luminosity as long as the damping is strong enough.

Figure 15 shows the average integrated luminosity as a function of the time in collisions, assuming a total turnaround time of $t_{\text{ta}} = 5$ h (as in [4]), evaluated with Eq. (31) and the results shown in the upper right plot

TABLE VII.   Initial IBS growth times for protons calculated with Piwinski's formalism, assuming the baseline lattice ($L_c = 203$ m). Assumption for momentum spread: injection $\sigma_p = 1.5 \times 10^{-4}$, collision (a) $\sigma_p = 0.5 \times 10^{-4}$ (obtained with γ_T of baseline lattice), (b) $\sigma_p = 1.1 \times 10^{-4}$ (LHC design).

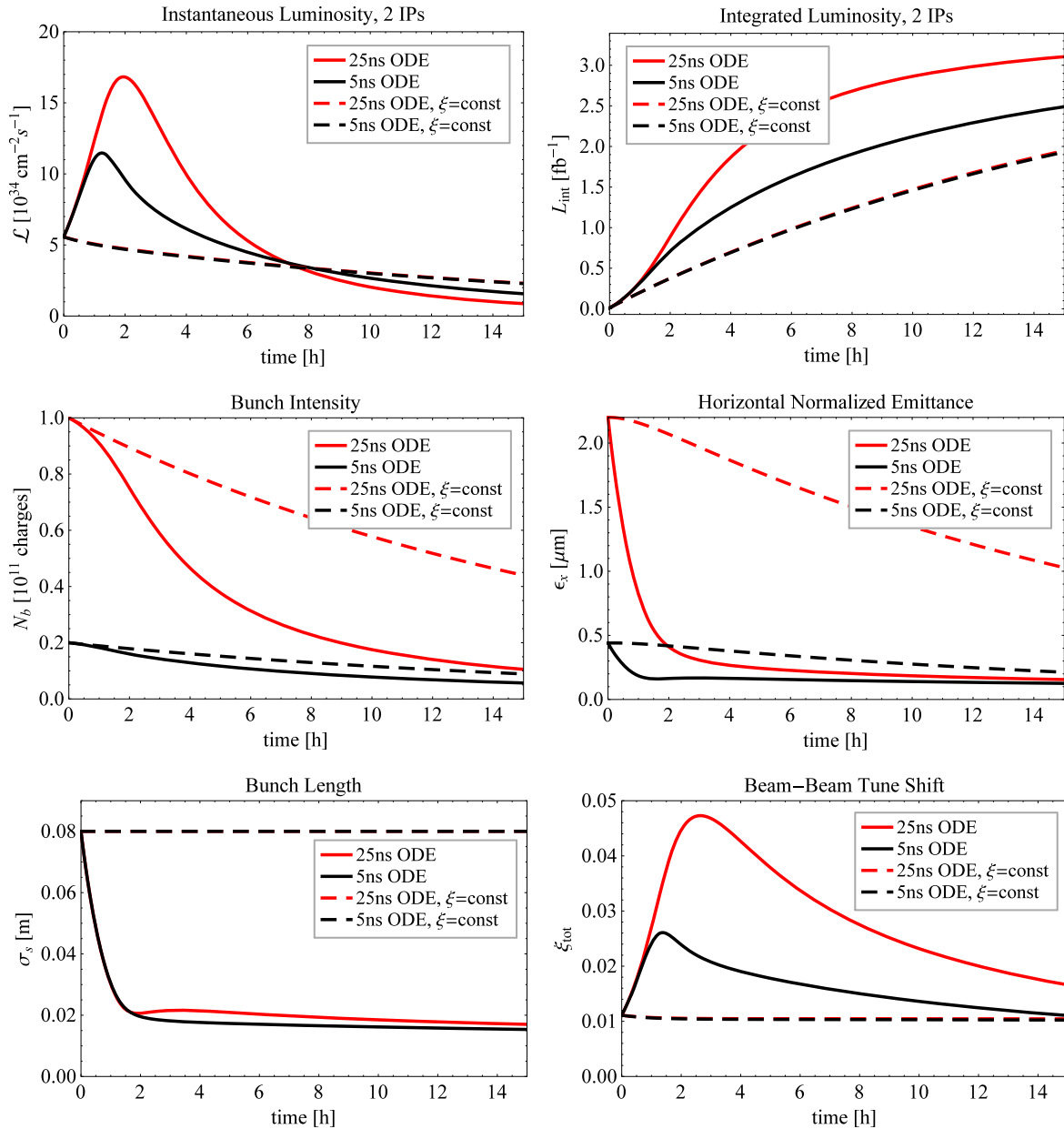| Growth Times | Unit | Injection | | Collision | | | |
| | | | | (a) | | (b) | |
		25 ns	5 ns	25 ns	5 ns	25 ns	5 ns
$1/\alpha_{\text{IBS},s}$	[h]	26.4	21.6	288.4	266.6	1480	1539
$1/\alpha_{\text{IBS},x}$	[h]	42.2	6.8	187.7	34.7	291.0	60.5
$1/\alpha_{\text{IBS},y}$	[h]	-10^6	-10^5	-10^7	-10^7	-10^8	-10^7

FIG. 14. *p-p* beam and luminosity evolution for two experiment in collisions. Top: instantaneous (left) and integrated (right) luminosity, middle: intensity (left) and normalized emittance (right), bottom: bunch length (left) and total beam-beam tune shift (right). Solid lines show free beam evolution without artificial blow-up, dashed lines show situation with constant bunch length and transverse emittance blow-up such $\xi = $ const. Beams for 25 (red) and 5 ns (black) bunch spacing are investigated. The instantaneous and integrated luminosity, the bunch length and tune shift evolution are very similar (overlapping lines) for both bunch spacings if $\xi = $ const.

of Fig. 14. The four cases discussed in the previous paragraph are displayed. The particle losses of proton bunches on the LHC injection plateau are small and thus neglected. The optimum time in collisions calculates to 5.5 h and 6.5 h for the 25 ns and 5 ns case of free beam evolution (solid lines), respectively. Under optimized conditions, 5.2 fb^{-1} (25 ns) and 3.5 fb^{-1} (5 ns) could be

(on average) collected per day. Considering $\xi = $ const, the two options are very similar. The integrated luminosity is maximized for 11.8 h collision time, delivering on average 2.3 fb^{-1}/day. If the beam-beam limit is higher than expected and the beams could be left to evolve freely, the luminosity outcome could potentially be doubled.
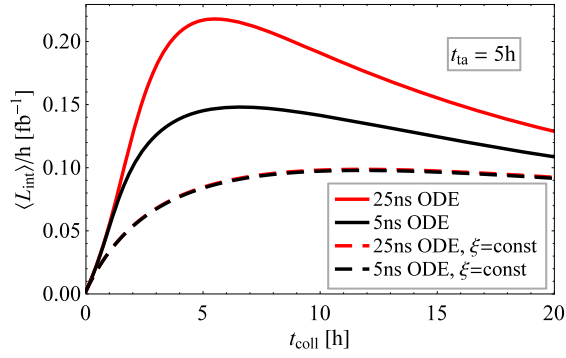
FIG. 15.   Average integrated luminosity per hour in $p - p$ operation.

VI. SUMMARY TABLE

In Table VIII calculated and assumed parameters for Pb-Pb, p-Pb and p-p operation at $E_b = 50Z$ TeV in the FCC-hh are summarized. In case of p-Pb operation the Pb beam is assumed to be the same as for Pb-Pb, therefore the corresponding column only quotes the proton beam parameters. The Pb beam parameters at injection are listed as well as the LHC Pb-Pb and p-p design parameters [8]. The p-p luminosity parameters given are based on the case where the beam-beam tune shift is kept constant to its initial value. The "/" separates the results for two beam options.

TABLE VIII.   Summary table.

		LHC		FCC		FCC	
	Unit	Design		Injection		Collision	
Operation mode	$\cdots$	*p-p*	Pb-Pb	Pb	Pb-Pb	*p*-Pb	*p-p* (25 ns/5 ns)
General storage ring parameters							
Circumference	[km]	26.659		100		100	
Field of main bends	[T]	8.33		1.0		16	
Bending radius	[m]	2803.95		10424		10424	
Cell length	[m]	106.9		203		203	
Gamma transition γ_T		55.7		103		103	
Revolution frequency	[kHz]	11.245		2.998		2.998	
rf frequency	[MHz]	400.8		400.8		400.8	
Harmonic number		35640		133692		133692	
Total rf voltage	[MV]	16		13		32	
Synchrotron frequency	[Hz]	23.0		8.4		3.4	
General beam parameters							
Beam energy	[TeV]	7	574	270	4100	50	50
Relativistic γ-factor		7461	2963.5	1397	21168	53290	53290
Number of bunches	$\cdots$	2808	592	432	432	432	10600/53000
Number of particles per bunch	[10^8]	1150	0.7	1.4	1.4	115	1000/200
Transverse normalised emittance	[μm.rad]	3.75	1.5	1.5	1.5	3.75	2.2/0.44
rms bunch length	[cm]	7.55	7.94	10.0		8.0	
rms energy spread	[10^{-4}]	1.129	1.1	1.9		0.6	
Longitudinal emittance (4 σ)	[eVs/charge]	2.5	2.5	2.6		10.1	
Circulating beam current	[mA]	584	6.12	2.38	2.38	2.38	509.14
Stored beam energy	[MJ]	362	3.8	2.6	39.8	39.8	8491.5
Intrabeam scattering and synchrotron radiation							
Longitudinal IBS emittance growth time	[h]	61	7.7	6.5	29.9	5×10^3	288.4/266.6
Horizontal IBS emittance growth time	[h]	80	13	11.2	33.4	5×10^3	187.7/34.7
Longitudinal emittance radiation damping time	[h]	13	6.3	852	0.24	0.5	0.5
Horizontal emittance radiation damping time	[h]	26	12.6	1704	0.49	1.0	1.0
Power loss per ion	[W]	1.8×10^{-11}	2.0×10^{-9}	1.1×10^{-11}	5.7×10^{-7}	3.4×10^{-9}	3.4×10^{-9}
Power loss per length in main bends	[W/m]	0.206	0.005	1.0×10^{-5}	0.53	0.26	55.4
Energy loss per ion per turn	[MeV]	0.007	1.12	0.01	775.3	4.7	4.7
Synchrotron radiation power per ring	[W]	3.6×10^3	83.9	0.7	34389	17016	3.6×10^6
Luminosity							
β-function at the IP	[m]	0.55	0.5	$\cdots$		1.1	
Initial rms beam size at IP	[μm]	16.7	15.9	$\cdots$	8.8	8.8	6.7/3.0

(Table continued)

TABLE VIII. (*Continued*)

	Unit	LHC		FCC	FCC		
		Design		Injection	Collision		
Number of IPs in collision	-	2 + 2	1	···	1	1	2
Crossing-angle	$[\mu\text{rad}]$	±142.5	0	···		0	
Initial luminosity	$[10^{27}\ \text{cm}^{-2}\,\text{s}^{-1}]$	10^7	1	···	2.6	213	5.6×10^7
Peak luminosity	$[10^{27}\ \text{cm}^{-2}\,\text{s}^{-1}]$	10^7	1	···	7.5	1240	5.6×10^7
Integrated luminosity per fill	$[\mu\text{b}^{-1}]$	···	<15	···	58.7	21648	1.65×10^9
Average integrated luminosity/hour	$[\mu\text{b}^{-1}]$	···	···	···	11.7	2547	98.2×10^6
Optimum time in collision	[h]	···	···	···	3.0	6.5	11.8
Assumed turnaround time	[h]	···	···	···	2.0	2.0	5.0
Initial beam-beam tune shift per IP	$[10^{-4}]$	33	1.8	···	3.7	3.7	55.5
Total cross-section	[b]	0.1	515	···	597	2	0.153
Peak BFPP beam power	[W]	0	26	···	1751	0	0

VII. CONCLUSIONS

The FCC will enter a new regime of hadron collider operation. Strong radiation damping will lead to small emittances and very efficient intensity burn-off. The emittances and bunch length become so small that artificial blow-up might be necessary to avoid instabilities. An artificial blow-up might also be used as a way of luminosity leveling. Because of the small beam dimensions, the peak Pb-Pb luminosity can be expected to be about 7 times the nominal LHC design value. The absolute integrated luminosity maximum per fill, when all particles are converted into luminosity, comes into reach, again because of the natural cooling from radiation damping. It is estimated that an integrated luminosity of about 8 nb^{-1} could be expected per run of 30 days.

If the LHC is used as the last preaccelerator, its cycle time has to be drastically improved. Otherwise, the time between two injections into the FCC will be in the same order as the expected time in collisions per fill. To optimize the run time, the LHC could be refilled in parallel to physics operation, maximizing the time in physics and the integrated luminosity, while filling only one fourth of the FCC.

In p-Pb operation, the fill length is determined by the burn-off of the lead beam. The longer radiation damping time and weaker IBS of the proton beam, lead to longer fills in p-Pb operation. However, by adjusting the proton beam intensity the luminosity peak and time distribution could be leveled.

The formalisms developed for the heavy-ion operation have also been applied to p-p operation. First prediction of the p-p beam and luminosity evolution, under the assumption of constant bunch length and an emittance blow-up, designed to keep the beam-beam tune shift $\xi = \text{const}$, have been presented. Furthermore, IBS calculations show that transverse emittance growth for long injection plateaus could become an issue for high intensity, low emittance protons.

[1] C. O. Dominguez and F. Zimmermann, Beam parameters and luminosity time evolution for an 80-km VHE-LHC, in *Proceedings of the 4th International Particle Accelerator Conference, IPAC- 2013, Shanghai, China, 2013* (JACoW, Shanghai, China, 2013), p. 1442, http://accelconf.web.cern.ch/AccelConf/IPAC2013/papers/tupfi042.pdf.

[2] N. Armesto, A. Dainese, D. d'Enterria, S. Masciocchi, C. Roland, C. A. Salgado, M. van Leeuwen, and U. A. Wiedemann, Heavy-ion physics studies for the future circular collider, Nucl. Phys. A **931**, 1163 (2014).

[3] R. Bruce, J. M. Jowett, M. Blaskiewicz, and W. Fischer, Time evolution of the luminosity of colliding heavy-ion beams in BNL relativistic heavy ion collider and CERN large hadron collider, Phys. Rev. ST Accel. Beams **13**, 091001 (2010).

[4] A. Ball *et al.*, Future circular collider study, hadron collider parameters, CERN Report No. FCC-ACC-SPC-0001, 2014.

[5] R. Alemany Fernandez and B. Holzer, First considerations on beam optics and lattice design for the future hadron-hadron collider FCC, CERN Report No. CERN-ACC-NOTE-2014-0065, 2014.

[6] *Handbook of Accelerator Physics and Engineering*, 2nd ed., edited by A. Chao, K. Mess, M. Tigner, and F. Zimmermann (World Scientific, Singapore, 2013).

[7] H. Wiedemann, *Particle Accelerator Physics*, 3rd ed. (Springer, New York, 2007).

[8] LHC design report volume I - The LHC main ring, CERN Report No. CERN-2004-003-V-1, 2004.

[9] V. N. Litvinenko *et al.*, Experience with IBS-suppression lattice in RHIC, in *Proceedings of the 11th European Particle Accelerator Conference, Genoa, 2008* (EPS-AG, Genoa, Italy, 2008), p. 2557.

[10] M. Schaumann and J. M. Jowett, Bunch-by-bunch analysis of the LHC heavy-ion luminosity, in *Proceedings of the 4th International Particle Accelerator Conference, IPAC-2013, Shanghai, China, 2013* (JACoW, Shanghai, China, 2013), p. 1391.

[11] J. Jowett, R. Alemany-Fernandez, P. Baudrenghien, D. Jacquet, M. Lamont, D. Manglunki, S. Redaelli, M. Sapinski, M. Schaumann, M. S. Camillocci, R. Tomás, J. Uythoven, D. Valuch, R. Versteegen, and J. Wenninger, Proton-nucleus collisions in the LHC, in *Proceedings of the 4th International Particle Accelerator Conference, IPAC-2013, Shanghai, China, 2013* (JACoW, Shanghai, China, 2013), p. 49.

[12] M. Schaumann, Heavy-ion performance of the LHC and future colliders , Ph.D. thesis, RWTH Aachen University, Aachen, Germany (to be published).

[13] M. Schaumann, Semi-empirical model for optimising future heavy-ion luminosity of the LHC, in *Proceedings of the 5th International Particle Accelerator Conference, IPAC-2014, Dresden, Germany, 2014* (JACoW, Dresden, Germany, 2014), p. 1033.

[14] J. Wei, A. Fedotov, W. Fischer, N. Malitsky, G. Parzen, and J. Qiang, Intra-beam scattering theory and RHIC experiments, AIP Conf. Proc. **773,** 389 (2005).

[15] A. Piwinski, Intra-beam scattering, in *Proceedings of the IXth International Conference on High Energy Accelerators, Stanford Linear Accelerator Center, Stanford, CA, USA, 1974, CONF-740522* (NTIS, Springfield, 1974), p. 405.

[16] J. Bjorken and S. Mtingwa, Intrabeam scattering, *Part. Accel.* **13,** 115 (1983).

[17] K. L. F. Bane, H. Hayano, K. Kubo, T. Naito, T. Okugi, and J. Urakawa, Intrabeam scattering analysis of measurements at KEK's accelerator test facility damping ring, Phys. Rev. ST Accel. Beams **5,** 084403 (2002).

[18] S. Nagaitsev, Intrabeam scattering formulas for fast numerical evaluation, Phys. Rev. ST Accel. Beams **8,** 064403 (2005).

[19] J. Wei, Evolution of hadron beams under intrabeam scattering, in *Proceedings of the 15th Particle Accelerator Conference, PAC-1993, Washington, DC, 1993* (IEEE, New York, 1993), p. 3651.

[20] A. Piwinski, Intra-beam scattering, in *CAS—CERN Accelerator School: Accelerator Physics, Oxford, UK (CERN, Oxford, UK, 1985), p. 402;* Report No. CERN-1987-003-V-1.402.

[21] H. Meier, Z. Halabuka, K. Hencken, D. Trautmann, and G. Baur, Bound-free electron-positron pair production in relativistic heavy-ion collisions, Phys. Rev. A **63,** 032713 (2001).

[22] H. H. Braun, A. Fassò, A. Ferrari, J. M. Jowett, P. R. Sala, and G. I. Smirnov, Hadronic and electromagnetic fragmentation of ultrarelativistic heavy ions at LHC, Phys. Rev. ST Accel. Beams **17,** 021006 (2014).

[23] J. M. Jowett, H. Braun, M. Gresham, E. Mahner, A. Nicholson, I. Pshenichnov, and E. Shaposhnikova, Limits to the performance of the LHC with ion beams, in *Proceedings of the 9th European Particle Accelerator Conference, Lucerne, 2004* (EPS-AG, Lucerne, 2004), p. 578, http://accelconf.web.cern.ch/AccelConf/e04/.

[24] W. Fischer, A. J. Baltz, M. Blaskiewicz, D. Gassner, K. A. Drees, Y. Luo, M. Minty, P. Thieberger, M. Wilinski, and I. A. Pshenichnov, Measurement of the total cross section of uranium-uranium collisions at $\sqrt{sNN} = 192.8$ GeV, Phys. Rev. C **89,** 014906 (2014).

[25] K. Hübner and E. Keil, Optimisation of average luminosity in pp and $\bar{p}p$ colliders, IEEE Trans. Nucl. Sci. **32,** 1632 (1985).

[26] M. Schaumann, Beam-beam interaction studies at LHC, Master's thesis, RWTH Aachen University, Aachen, Germany (2011); Report No. CERN-THESIS-2011-138.

[27] A. J. Baltz, M. J. Rhoades-Brown, and J. Weneser, Heavy-ion partial beam lifetimes due to Coulomb induced processes, Phys. Rev. E **54,** 4233 (1996).

[28] R. Bruce, D. Bocian, S. Gilardoni, and J. M. Jowett, Beam losses from ultraperipheral nuclear collisions between ^{208}Pb^{82+} ions in the Large Hadron Collider and their alleviation, Phys. Rev. ST Accel. Beams **12,** 071002 (2009).

[29] J. M. Jowett, M. Schaumann, and R. Versteegen, Heavy ion operation from Run 2 to HL-LHC, in *Proceedings of RLIUP: Review of LHC and Injector Upgrade Plans, Centre de Convention, Archamps, France*, edited by B. Goddard and F. Zimmermann (CERN, Geneva, 2014), CERN-2014-006.

[30] A. Zlobin *et al.*, Status of 11T 2-in-1 Nb3Sn dipole development for LHC, in *Proceedings of the 5th International Particle Accelerator Conference, IPAC-2014, Dresden, Germany, 2014* (JACoW, Dresden, Germany, 2014), p. 2722.

[31] R. Brinkmann and F. Willeke, First experience with colliding electron-proton beams in HERA, in *Proceedings of the 15th Particle Accelerator Conference, PAC-1993, Washington, DC, 1993* (IEEE, New York, 1993), p. 3742.

[32] K. Cornelis, M. Meddahi, and R. Schmidt, The beam-beam effect in the SPS proton anti-proton collider for beams with unequal emittances, CERN Report No. CERN SL/90-73 (AP), 1990.

[33] M. Syphers, Beam-beam tune distribution with differing beam sizes, Fermilab Report Nos. Fermilab-AD, Beams-doc-3031-v1, 2008.

[34] *Accelerator Physics at the Tevatron Collider*, edited by V. Lebedev and V. Shiltsev (Springer, New York, 2014).